Science of the Total Environment 905 (2023) 167091

Contents lists available at ScienceDirect

Science of the Total Environment

journal homepage: www.elsevier.com/locate/scitotenv

Effects of landscape on thermal livability at the community scale based on fine-grained geographic information: A case study of Shenzhen

Yue Liu [a], Xin Huang [b,c,*], Qiquan Yang [d], Wenlong Jing [a,e], Ji Yang [a,e]

[a] Guangzhou Institute of Geography, Guangdong Academy of Sciences, Guangzhou 510070, PR China
[b] School of Remote Sensing and Information Engineering, Wuhan University, Wuhan 430079, PR China
[c] State Key Laboratory of Information Engineering in Surveying, Mapping and Remote Sensing, Wuhan University, Wuhan 430079, PR China
[d] College of Surveying & Geo-Informatics, Tongji University, Shanghai 200092, PR China
[e] Southern Marine Science and Engineering Guangdong Laboratory (Guangzhou), Guangzhou 511485, PR China

HIGHLIGHTS

- A land surface temperature (LST) threshold was used to assess the thermal livability.
- Building height and tree coverage dominantly affected the average community LST.
- Building morphology mainly determined the spatial distribution of community LST.
- About 20 % tree coverage and 40–60 m building height can cool the community LST most.
- Thermally livable communities have higher volume ratio and lower sky view factor.

GRAPHICAL ABSTRACT

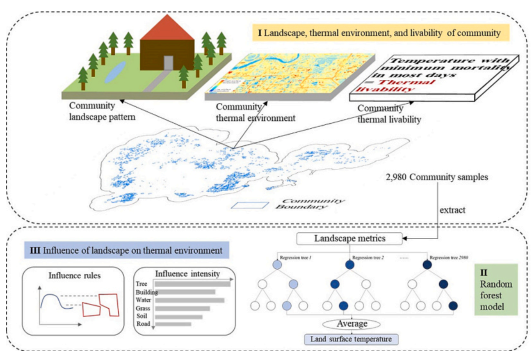

ARTICLE INFO

Editor: Shuqing Zhao

Keywords:
Community planning
Landscape structure
Urban microclimate
Thermal livability
Urban renewal

ABSTRACT

In the current research, the question of how to modify the microclimate through landscape planning to create a livable thermal environment within a residential community area has not been clarified. Therefore, this study investigated the effects of landscape on thermal livability in 2980 communities in Shenzhen, and obtained the following findings: (1) the proportion of trees and the average building height were key indicators to determine the average land surface temperature (LST) of a community, while the two-dimensional building characteristics, particularly shape, similarity, and patch dominance, were mainly responsible for regulating the spatial distribution of LST within a community; (2) at the community scale, the cooling intensity of buildings was strongest when their average height was around 40-60 m, and cooling effect of trees was most pronounced when their proportion achieved 20 %; and (3) the LST threshold for thermal livability in Shenzhen was around 35 °C. In summer, a higher proportion of trees and grass, as well as buildings with higher average heights, larger volume ratios, and more complex three-dimensional structures were favorable to maintain a livable community thermal environment, while in winter, a lower proportion of trees was more encouraged. In addition, a smaller average sky view factor can achieve a community thermal environment that warm in winter and cool in summer. These

* Corresponding author at: School of Remote Sensing and Information Engineering, Wuhan University, Wuhan 430079, PR China.
E-mail addresses: yliu_rs@whu.edu.cn (Y. Liu), xhuang@whu.edu.cn (X. Huang), qiquanyang@tongji.edu.cn (Q. Yang), jingwl@Ireis.ac.cn (W. Jing), yangji@gdas.ac.cn (J. Yang).

https://doi.org/10.1016/j.scitotenv.2023.167091
Received 2 June 2023; Received in revised form 23 August 2023; Accepted 13 September 2023
Available online 15 September 2023

results are expected to facilitate urban planners to develop community renewal from the perspective of thermal livability.

1. Introduction

The urban warming induced by urbanization has been a widespread concern. Some abnormal temperature events (e.g., heat waves, cold waves, etc.) pose risks to the physical and psychological health of residents, especially for those who are engaged in outdoor production activities (Deschenes, 2014). Given the fact that urbanization development is inevitable, how to regulate and improve the urban thermal environment as much as possible through landscape planning is an urgent issue for current research.

Landscape planning has been regarded as a globally adaptation strategy to improve outdoor thermal comfort in cities. The United States promulgated a series of regulations on landscaping to mitigate land surface temperature (LST) and seek sustainable construction patterns (Larson et al., 2020). Similarly, China (Yao et al., 2020), Japan (Xiao and Yuizono, 2022) and South Korea (Kim et al., 2020) improved their outdoor thermal comfort by optimizing green landscape layout mode. In addition, the building landscape also plays an important role in climate adaptation planning networks. During 2016 to 2022, the Tokyo Metropolitan Resilience Plan and the Tokyo Disaster Prevention Plan successively proposed a "design of the built environment" strategy to mitigate extreme heat through spatial planning and design interventions (Kim et al., 2022a). Evidence from different regions suggested that the urban thermal environment can be effectively improved by adjusting landscape configurations (referring to the composition, structure, and distribution pattern of landscapes) (Ramyar et al., 2021). As a corollary, rational landscape configurations have great potential to create the "microclimate refuge" in cities, i.e., a small patch buffered from climate change due to their less exposure to extreme temperatures and external fluctuations (Keppel et al., 2017). Microclimate refuges can provide relatively comfortable living environments for residents when they have difficulty adapting in climate change scenarios (Suggitt et al., 2018).

Community, as the basic unit of urban settlements, is undoubtedly the best place to create the urban microclimate refuge (Hsu et al., 2021). Since 2020, China has been promoting the Community-oriented Micro-renewal Project (Tang et al., 2022). Through renovating the community landscapes, the livability of many old communities can be evidently improved. The goal of "livability" focuses on creating comfortable living spaces to meet the aspirations of community residents for a better life (Ruth and Franklin, 2014). However, community livability mentioned in existing studies mainly involved the building environment, ecological livability, transportation convenience, living comfort, and security (Huang and Liu, 2022), while little attention has been paid to the livability of thermal environment (in this paper, referred to as "thermal livability"). Accurately understanding the effects of landscape on the thermal environment at the community scale is a prerequisite for scientifically improving the community thermal livability, which is also one of the main research objectives of this study.

Another objective of this study is to quantitatively explore landscape configurations that are conducive to creating thermally livable communities. The first issue that needs to be clarified is what kind of community can be called a thermally livable community. Since the 20th century, researchers have successively developed >165 thermal comfort indices to assess the indoor and outdoor thermal environments (de Freitas and Grigorieva, 2017). These indices were designed to estimate the energy exchange between the surrounding environment and the human body based on thermodynamic principles, which took into account basic environmental parameters such as humidity, air temperature, air velocity, radiation temperature, type of activity and the insulating properties of the subject's clothing (Kumar and Sharma, 2020). However, the thermal comfort index is inadequate when applied to assess the thermal livability. First, a "livable" thermal environment should be both comfortable and stable, but the traditional thermal comfort index can only be used to characterize the instantaneous comfort of a thermal environment without considering its temporal and spatial variations. Secondly, the calculation of the thermal comfort index requires the input of a large number of meteorological parameters measured by the ground in real time, which is not conducive to the large-scale and high-frequency assessment of the thermal livability. In this regard, a new thermal livability index based on LST values that retrieved from remotely sensed images will better solve these problems, because remote sensing data often have higher spatial and temporal resolution and do not depend on in situ measurements (Zhou et al., 2018; Yang et al., 2023).

Overall, in recent years, the effect of landscape configurations on the thermal environment has been widely discussed at the macro scale (Zhou et al., 2016; Yao et al., 2017; Wang et al., 2019; Yang et al., 2021), but at the micro scale, especially at the community scale with exclusive residential functions, the related studies were comparatively rare. Also, few studies have directly linked landscape configurations with thermal livability. Although LST is an indirect proxy for the thermal environment (Kim et al., 2022a), how it can be used to measure thermal livability remain largely unknown.

Therefore, this study introduced a wide range of fine-grained geographic datasets, including 2.1 m high-resolution remote sensing imagery, very high-resolution light detection and ranging (LiDAR) data, 30-m-resolution LST data products and the boundaries of individual communities, to produce landscape maps and building height maps within 2980 communities in Shenzhen, with the aims of: (1) clarifying the influence intensity, influence rules and their temporal variations of the landscape configurations on thermal environment at the community scale; and (2) assessing the livability of each community's thermal environment by designing a LST-based thermal livability index, so as to specifically and quantitatively analyze what kind of landscape configurations are conducive to maintaining a livable community thermal environment.

2. Study area

In this study, Shenzhen, Guangdong Province, China, was selected as a representative study area (Fig. 1). As China's first special economic zone, Shenzhen has been at the forefront of the world in urban construction, especially in community construction, so the study of the community-scale landscapes and thermal livability in this city is expected to be transformed into practical planning policies that can serve as an exemplary role for other cities to create thermally livable communities.

Considering the distribution characteristics of the urban heat island effect, this study confined the research scope to the main urban area of Shenzhen. The boundary of the main urban area was delineated as follows (Zhou et al., 2015): (1) establishing a 1 km $\times$ 1 km grid on the ZiYuan-3 high-resolution land cover map (see Section 3.1); (2) dividing each grid into a high-density grid (>50 %) and a low-density grid (<50 %) based on the density of buildings (DOB) in each grid; and (3) merging the high-density grid and generating a 2 km buffer zone at its periphery to obtain the final boundary of the main urban area.

The acquisition of community boundaries included three steps: (1) downloading point-of-interest (POI) data labeled as residential areas from the open API interface provided by Baidu Map platform and cleaning the data; (2) obtaining the corner point information of area-of-interest (AOI) boundary corresponding to the POIs; and (3) vectorizing the AOIs in geographic data processing software (e.g., ArcGIS, QGIS) and conducting geographic correction and topology checking. After the above processing, a total of 3306 community boundaries were extracted. Then, these communities were further filtered by removing those without available fine-grained geographic data, and those with areas smaller than a pixel size of LST data. Finally, 2980 communities located in the main urban area were retained for this study. These communities are between 1363.27 m^2–514,150.31 m^2 in size and their spatial distribution is shown in Fig. 1.

3. Data acquisition and processing

3.1. High-resolution land cover map

To meet the needs of community-scale research, this study used ZiYuan-3 high-resolution remote sensing imagery for land cover mapping. The data were mainly collected from the China Natural Resources Satellite Remote Sensing Cloud Service Platform (http://sasclouds.com/chinese/normal/). ZY-3 is the first civil high-resolution stereo mapping satellite constellation in China, consisting of two satellites, ZY-3 01 and ZY-3 02 (Tang et al., 2015). Each satellite carries four optical sensors with 22° positioning, including one nadir-view panoramic camera, two side-view panoramic cameras (forward-view and backward-view), and one ortho-optical multispectral camera with spatial resolutions of 2.1 m, 2.5 m, and 5.8 m, respectively (Huang and Wang, 2019).

The ZY-3 satellite images were acquired during the limited period of April to October 2013 and with cloud cover <30 %. In this study, seven representative urban land cover categories were extracted, including: grass, tree, bare soil, building, water body, road, and other open impervious surface (OIS). The mapping process was shown in Fig. 2, and detailed methods could be referred to Huang et al. (2020).

Firstly, all remote sensing images were pre-processed: (1) fusing nadir-view and forward-view image pairs to generate a Digital Surface Model (DSM) of the main urban area, and then producing orthogonal products of nadir-view images based on this DSM; (2) fusing the multispectral image with the orthorectified nadir-view image to improve its spatial resolution to 2.1 m; and (3) registering the auxiliary data with reference to the coordinate system of multispectral image.

Secondly, buildings, roads and water objects were extracted from the auxiliary data: (1) obtaining building footprints mainly from Gaode Map platform, supplemented by the Map World data; (2) obtaining road networks main from Open Street Map, supplemented by the Map World data; and (3) obtaining water body boundaries from Map World data. All objects in the data that were inconsistent with the ZY-3 satellite image had been manually adjusted.

Thirdly, grass, trees, bare soil and OIS were extracted from the remaining areas of the images: (1) calculating normalized difference vegetation index (NDVI), normalized difference moisture index (NDWI), multispectral features and normalized DSM values based on the multispectral images and DSM data; (2) inputting the above variables into a random forest model for classification, where the ratio of training samples to testing samples was about 8:1; and (3) artificially correcting the classification results with reference to Google Earth images.

Finally, the accuracy of classification results was evaluated Fig. 3 showed the land cover mapping results of the main urban area of Shenzhen. Qualitatively, the mapping result clearly depicted the contour information of different land cover types, especially some small and mixed buildings and vegetation landscapes, and the continuous linear pattern of roads was well preserved. Quantitatively, the user accuracy and producer accuracy of all land cover types in the mapping results exceeded 85 %, with an overall accuracy of 88.38 % (Table S1), which can meet the requirements of our fine-grained studies.

3.2. Building height data

The building heights used in this study were extracted from the LiDAR point cloud data provided by Shenzhen Municipal Bureau of Planning and Natural Resources, which covered a total of 562, 257 single buildings within the main urban area (Fig. 4 (a)–(b)). To verify the data accuracy, we randomly selected 200 buildings from the data, and their reference height values were obtained by Google Street View map. Fig. 4 (c) showed the linear regression results between the data values and the reference values. The average R^2 and RMSE of the regression model were 0.95 and 0.42 m, respectively, implying that the data was reliable.

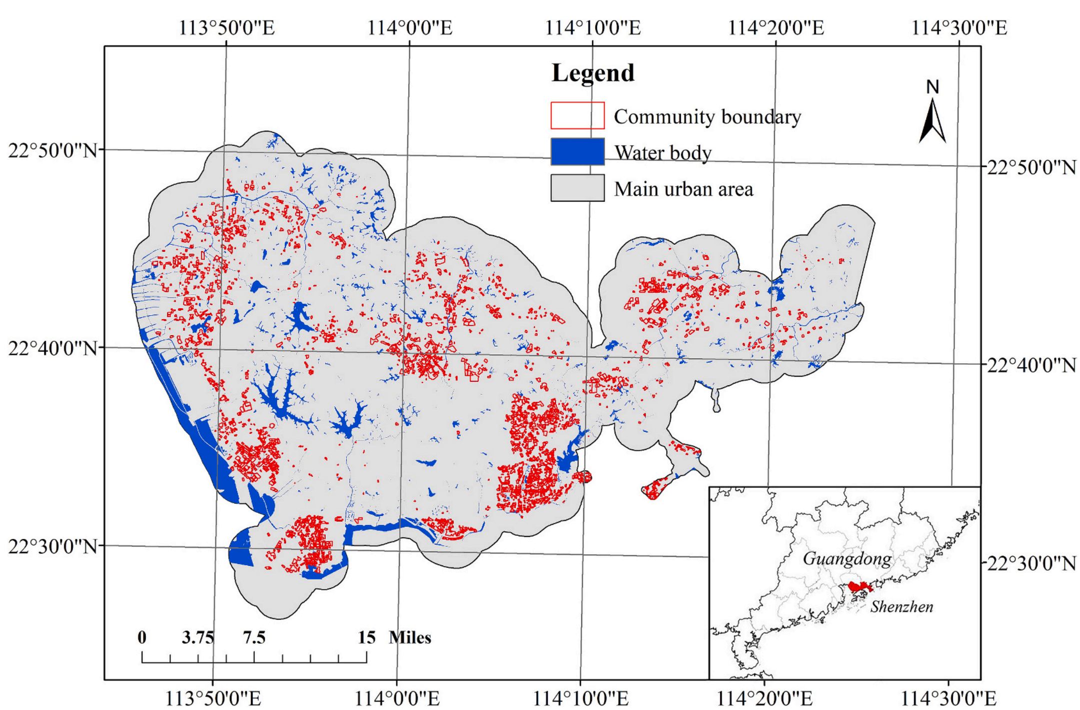

Fig. 1. Study area location and community distribution.

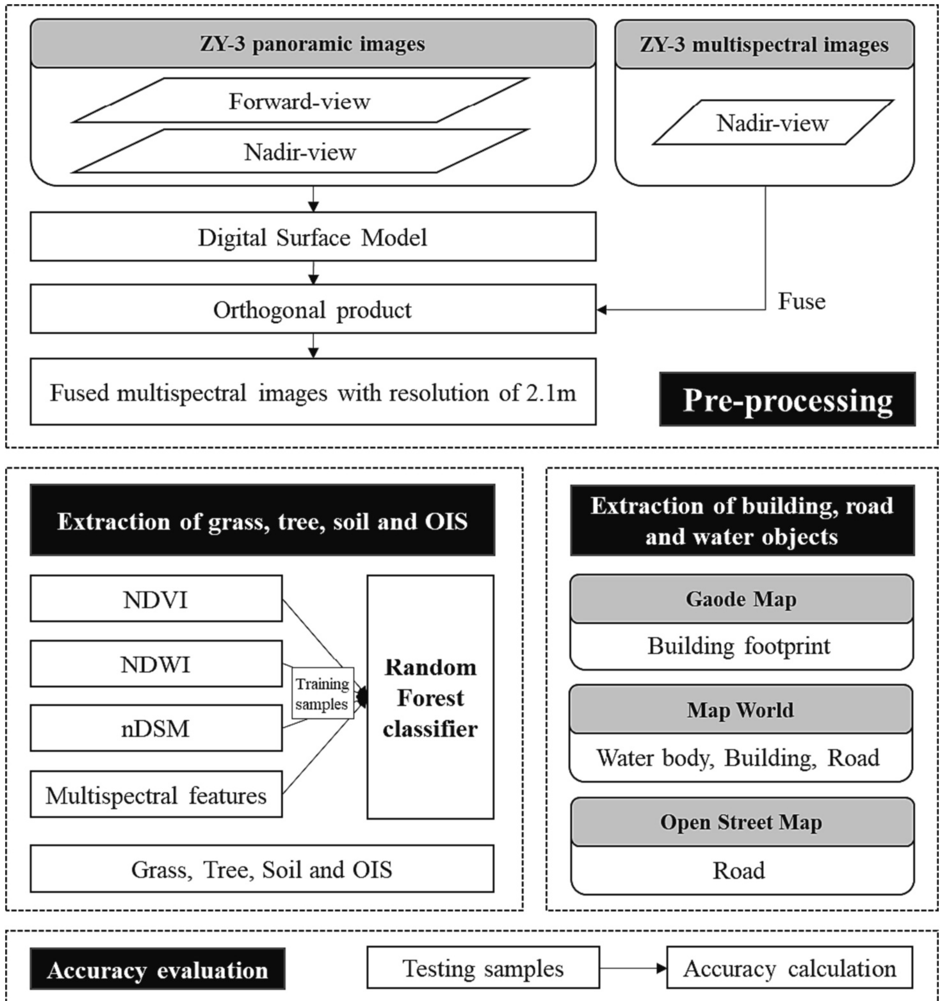

Fig. 2. The technical process of land cover classification and mapping based on ZY-3 images.

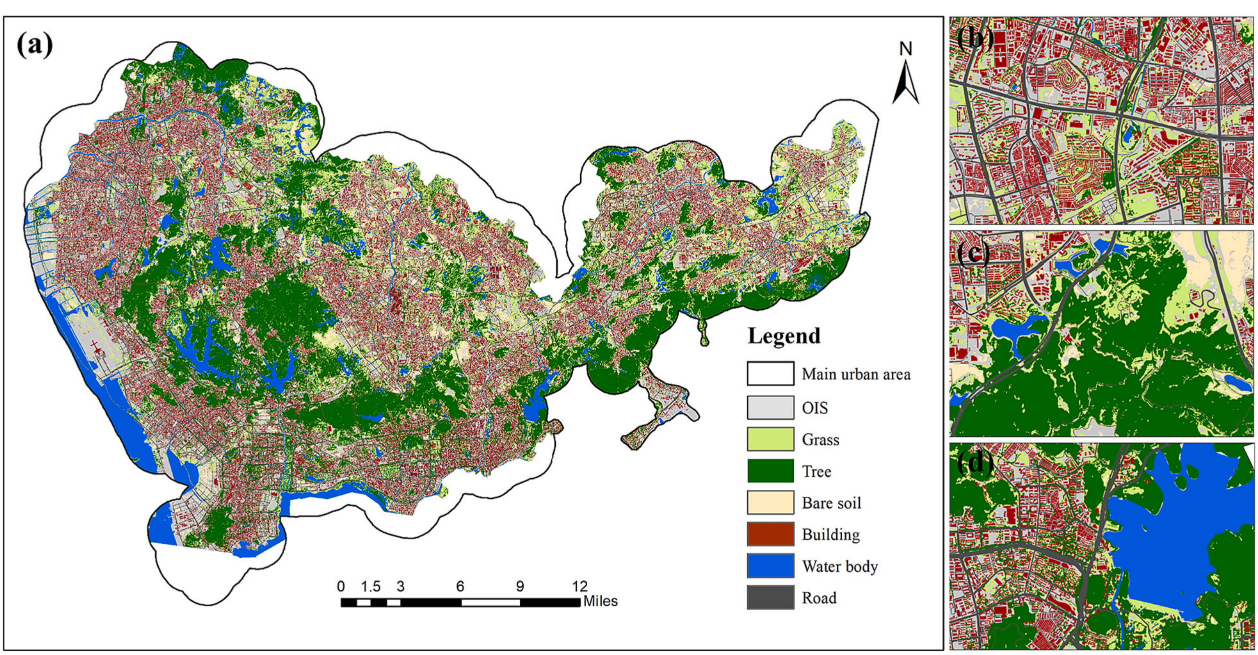

Fig. 3. Land cover mapping result based on ZY-3 high-resolution remote sensing images. (a): Global map; (b)–(d): Local details.

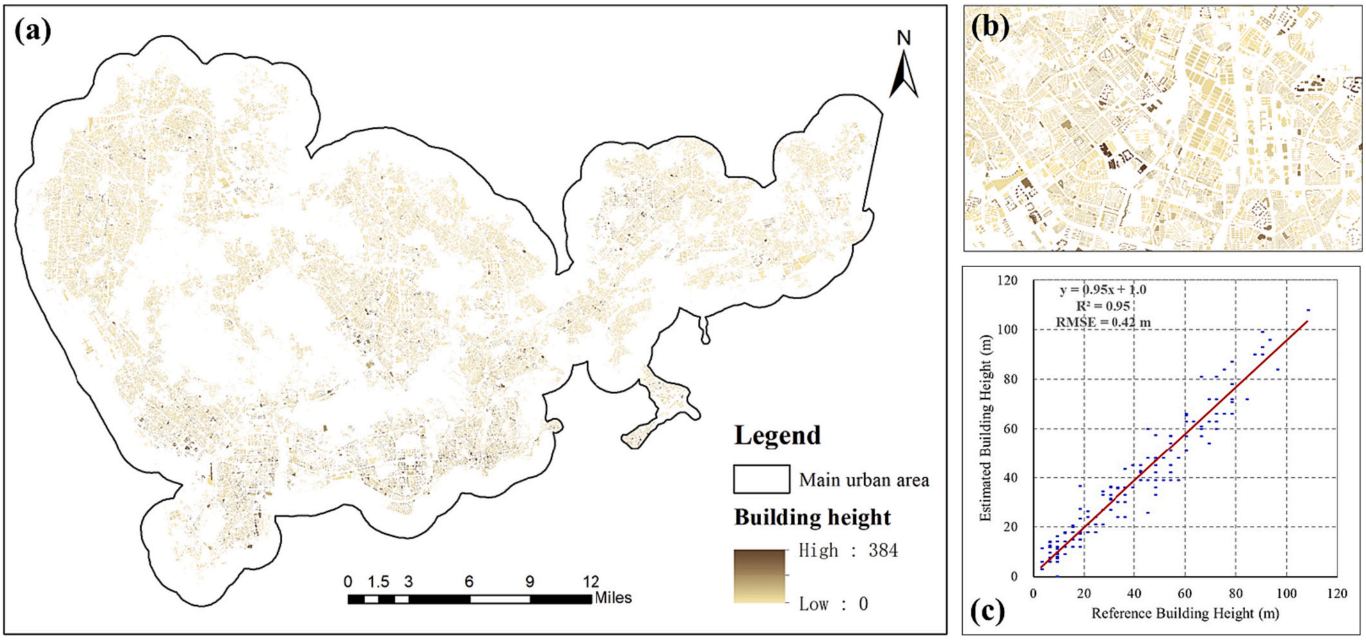

Fig. 4. Building height extracted from the laser point cloud data. (a): Global map; (b): Local details; (c) Accuracy evaluation.

3.3. Landscape metrics

Landscape metrics are effective tools for quantitatively describing the configurations (e.g., composition, structure and spatial pattern) of landscapes, which have been widely applicated in urban landscape studies (O'Neill et al., 1988; Turner, 1990). In order to comprehensively understand the landscape pattern of communities, a total of 155 metrics were selected in this study with reference to previous literature, covering five aspects such as area-edge, shape, core area, contrast, and aggregation. Among them, there were one two-dimensional (2D) composition metrics for each of seven landscape categories (tree, grassland, bare soil, building, water body, road, OIS), 47 2D structure metrics for each of three landscape categories (tree, grassland, building) and seven three-dimensional (3D) structure metrics for building landscapes. After Spearman's correlation analysis, metrics with correlations exceeding 0.8 were excluded, and 28 metrics were retained and calculated for subsequent analysis (Table 1, Fig. S1). A detailed explanation of these metrics can be found in the help manual of the FRAGSTATS v4 software (McGarigal et al., 2012).

As shown in Table 1, the 2D composition metrics indicated that OIS

Table 1
Statistical description of landscape metrics of 2980 communities in Shenzhen.

Class	Metrics	Minimum-Maximum	Mean	Standard deviation	Variance coefficient
2D landscape composition	The proportion of OIS (*PLAND_OIS*)	1.3–83.5	40.8	15.5	0.4
	The proportion of grass (*PLAND_GRASS*)	0.0–38.5	10.1	9.6	1.0
	The proportion of tree (*PLAND_TREE*)	0.0–48.0	6.7	9.3	1.4
	The proportion of bare soil (*PLAND_SOIL*)	0.0–15.4	0.3	1.8	6.5
	The proportion of building (*PLAND_BUILDING*)	8.9–77.9	35.6	11.9	0.3
	The proportion of water body (*PLAND_WATER*)	0.0–0.2	0.0	0.0	10.6
	The proportion of road (*PLAND_ROAD*)	0.0–29.8	6.5	6.5	1.0
2D landscape structure	Patch density of building (*PD*)	85.4–2919.2	589.0	435.6	0.7
	Largest patch index of building (*LPI*)	0.9–77.7	18.4	15.4	0.8
	Edge density of building (*ED*)	185.9–1620.1	777.5	299.7	0.4
	Landscape shape index of building (*LSI*)	1.2–16.3	3.9	2.6	0.7
	Average shape index of building (*SHAPE_MN*)	1.0–2.7	1.5	0.3	0.2
	Average circumference of building (*CIRCLE_MN*)	0.3–0.8	0.6	0.1	0.2
	Average contiguity of building (*CONTIG_MN*)	0.3–0.9	0.8	0.1	0.2
	Average proximity of building (*PROX_MN*)	0.0–217.3	21.1	30.8	1.5
	Average similarity of building (*SIMI_MN*)	11.4–2774.6	203.2	281.4	1.4
	Average cohesion of building (*COHESION_MN*)	84.2–99.6	94.6	2.9	0.0
	Aggregation index of building (*AI*)	79.8–99.3	91.2	4.3	0.1
	Area-weighted average perimeter-area ratio of grass (*PARA_AM_GRASS*)	0.0–19,047.6	4600.5	4139.9	0.9
	Splitting index of grass (*SPLIT_GRASS*)	0.0–147,549,609.0	376,595.1	5,010,633.4	13.3
	Area-weighted average perimeter-area ratio of tree (*PARA_AM_TREE*)	0.0–19,047.6	4264.1	4030.7	1.0
	Splitting index of tree (*SPLIT_TREE*)	0.0–866,772,481.0	711,246.6	16,772,826.6	23.6
3D building structure	Orientation variance of the building (*OV*)	0.0–69.8	21.0	19.7	0.9
	Average building height (*MEAN_HEIGHT*)	3.0–96.0	33.4	22.6	0.7
	The standard deviation of building height (*STD_HEIGHT*)	0.0–39.1	5.9	6.7	1.1
	The volume ratio of building (*PLOT RATIO*)	0.2–15.1	4.0	2.8	0.7
	Average shape coefficient of building (*MEAN_SC*)	1.0–2.3	1.1	0.2	0.2
	Average sky view factor of building (*MEAN_SVF*)	0.7–1.0	0.8	0.1	0.1

was the most dominant landscape type in most communities, with an average proportion of 40.8 %, followed by buildings (35.6 %), grass (10.1 %), trees (6.7 %) and roads (6.5 %), respectively, while the average proportion of bare soil and water bodies in these communities was almost 0. In terms of the 2D building structure metrics, except for the average proximity of buildings and the average similarity of buildings, the variance coefficients of all metrics did not exceed 1, implying that most of the 2D structures of buildings were relatively similar across communities. In contrast, there were significant inter-community differences for the 2D structure metrics of grass and trees, especially the splitting index of grass and the splitting index of tree. For the 3D building structure metrics, the variance coefficient suggested that inter-community differences were mainly in the standard deviation of building height (1.1) as well as the orientation variance of buildings (0.9). On average, the average building height and the standard deviation of building height were 33.42 m and 5.90 m, respectively, while the orientation variance of buildings, the volume ratio of building, the average shape coefficient of building and the average sky view factor of building were 21.0°, 4.0, 1.1 and 0.8, respectively.

3.4. Landsat surface temperature product

In this study, the Level-2 Surface Temperature Science Products (L2SPs) from Landsat-7 and Landsat-8 Collection-2 dataset were utilized to characterize the land surface thermal environment. Detailed data description can be found at https://www.usgs.gov/landsat-missions/landsat-collections. Due to the cloud cover problem of the original images and the severe scanline error of Landsat-7 images, the available data of L2SPs were limited (Fig. 5). Therefore, this study expanded the data acquisition period to 2012–2014 to increase the amount of available data while maintaining temporal consistency with the land cover data. The strips of the selected L2SPs ranged from paths 121, rows 44 to paths 122, rows 44 under the WRS2 type, with a total of 199 images that covering the Shenzhen city (even if it is only a part of the area). Then, these L2SPs were geo-registered, linearly transformed and clipped.

It should be noted that some images have incomplete coverage (e.g., Fig. 5 (a), (c), (d)) and some images have missing scanlines (e.g., Fig. 5 (a), (b)), so a "community sampling" strategy was adopted for each image, i.e., communities that could not be fully covered by L2SPs were deleted (e.g., areas ① and ② in Fig. 6), while communities that had complete L2SP data coverage were retained (e.g., areas ③ and ④ in Fig. 6). Then, the mean LST error values within each retained community boundary were calculated based on the quality control (QA) band of L2SPs. Communities with mean LST errors exceeding 5 K were removed to ensure that the LST data used were of high quality.

In this way, each L2SP corresponded to a different number of available communities. To avoid bias in the regression model results due to the small number of input community samples, this study finally reserved 86 out of 199 L2SPs (Fig. 7), each of which corresponded to >100 available communities. Among them, there were no eligible L2SPs

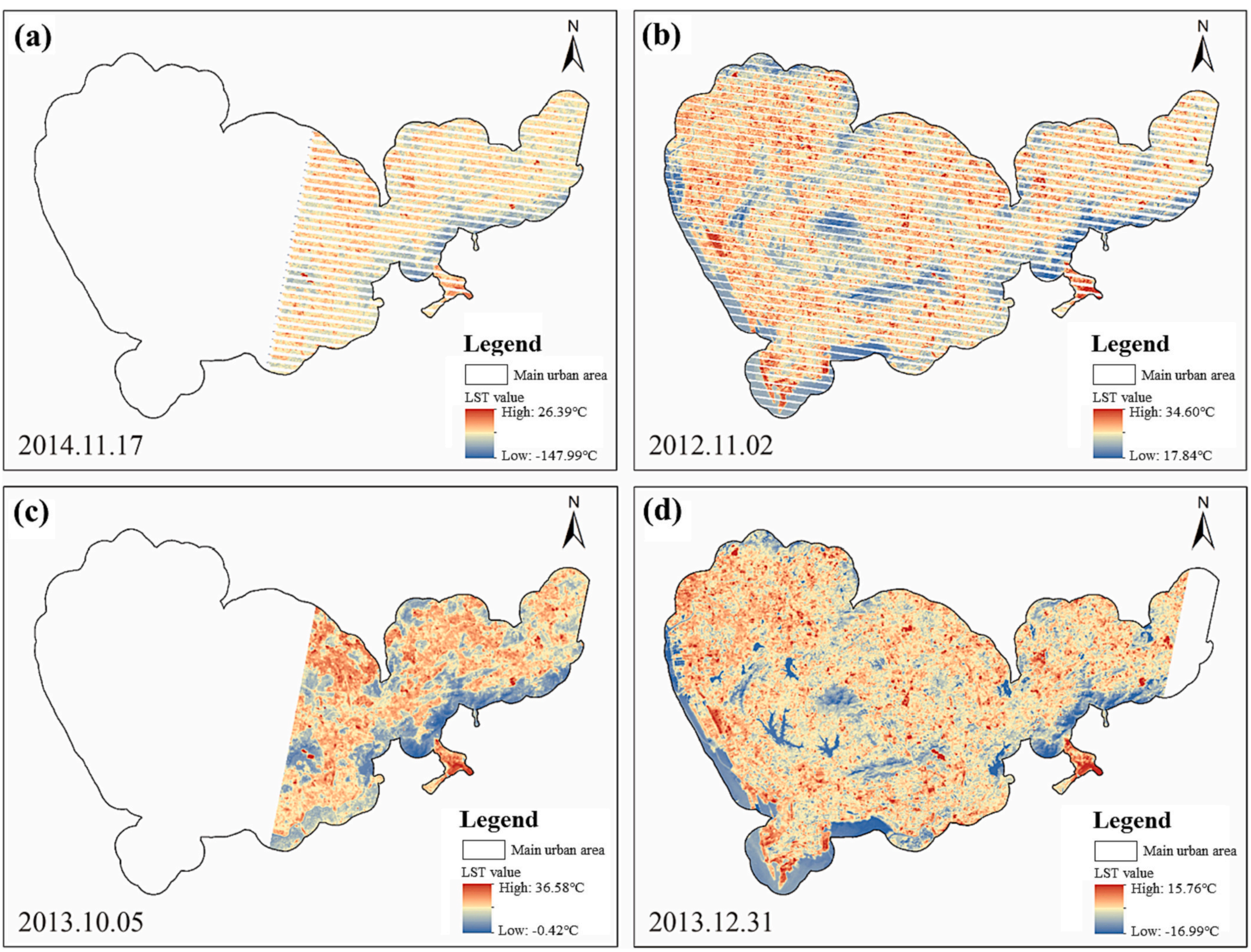

Fig. 5. Level-2 Surface Temperature Science Products (L2SPs) from Landsat Collection-2 dataset. (a): Landsat 7 (Path: 121, Row: 44); (b): Landsat 7 (Path: 122, Row: 44); (c): Landsat 8 (Path: 121, Row: 44); (d): Landsat 8 (Path: 122, Row: 44).

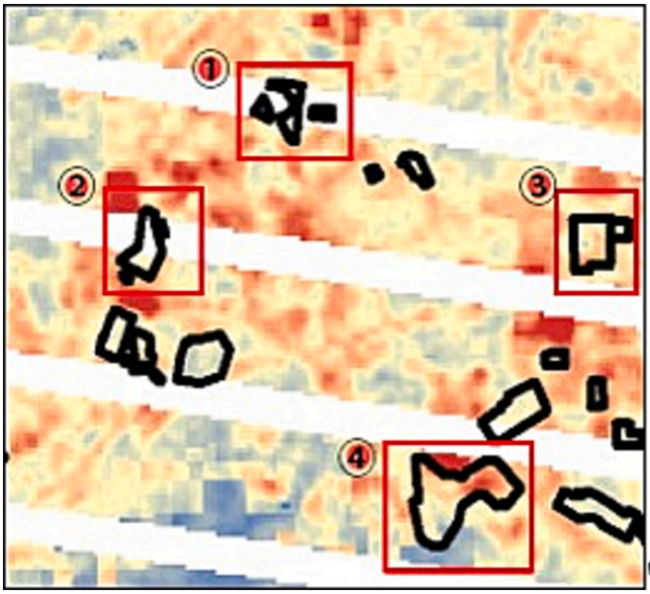

Fig. 6. Illustration of the "community sampling" strategy.

available in April due to severe cloud coverage problem, and only very few available data in March and May.

Finally, the accuracy of the L2SPs was validated against the daily average surface (0 cm) temperature recorded in the day-by-day meteorological data provided by the China Meteorological Administration for the years 2012–2014 (Fig. 8). Statistically, the difference between the average L2SPs and the meteorological data ranged from −7.46 °C (date: 20130105) to 3.34 °C (date: 20140516) for the 86 L2SPs, with a mean deviation of −2.74 °C, implying that the vast majority of the L2SPs value were lower than the meteorological value. This can be ascribed to the fact that the surface radiation received by satellite sensors will be absorbed and scattered by the atmosphere, resulting in the LST retrieved from remote sensing being slightly lower than its actual value. In general, the distribution pattern of daily LST averages from L2SPs and meteorological station data still showed a high degree of agreement.

As displayed in Fig. 8, the average LST values of 2980 communities ranged from 8.43 °C (date: 20131223) to 36.38 °C (date: 20140704). At the same moment in each day, there was an evident variation of the average LST between communities, ranging from 5.96 °C (date: 20131224) to 17.47 °C (date: 20140516), which further confirmed that variability in community landscapes can lead to heterogeneity in thermal environments. Therefore, rational landscape design has great value in improving the thermal livability of a community.

3.5. LST threshold for thermal livability

Out of the study purpose of assessing "community thermal livability", an adaptive thermal livability threshold was designed. This threshold was estimated by the minimum mortality temperature (MMT) (i.e., the air temperature corresponding to the lowest population mortality rate) in Shenzhen, which could be used to characterize the most comfortable and desirable air temperature for residents (Gasparrini et al., 2015). Compared to the traditional thermal comfort indices, the MMT indicator has two advantages in measuring thermal livability: (1) it can be estimated by the most frequent temperature (MFT) that recorded in the daily temperature data of the weather station. Yin et al. (2019) have demonstrated that this estimation method was not only convenient but also highly accurate; and (2) it can be adjusted according to the climatic context of different regions to adapt to regional heterogeneity.

The daily mean temperature and the annual MFT in 2012, 2013 and 2014 were calculated based on the day-by-day meteorological data of Shenzhen from the China Meteorological Administration (Fig. 9). By averaging the MFT values for three years (29.51 °C, 28.55 °C, 29.60 °C), the MMT of Shenzhen was set to approximately 29 °C during the study period.

Then, the LST threshold for thermal livability was inferred from the MMT. A total of 20 L2SPs with <10 % cloud coverage in the main urban area were selected for comparison with the air temperature of the weather station on the same date, and a significant positive correlation was found between the maximum value of LST in each L2SP and the daily mean air temperature (Fig. 10 (a)). On average, the daily LST maximum is 5.59 °C higher than the daily air temperature, and this deviation tended to increase as the temperature increased (Fig. 10 (b)), which is in general agreement with the findings of many previous studies (Shiflett et al., 2017; Goldblatt et al., 2021; Cao et al., 2021). Based on these findings, in this study, the LST threshold for thermal livability was set roughly at MMT + 6 °C, i.e., 35 °C.

3.6. Random Forest model

A random forest (RF) regression model was introduced to analyze the community-scale effect of landscape on thermal livability. RF is a commonly used machine learning algorithm consisting of nonparametric ensemble methods that rely on classification and regression tree (CART) models (Breiman, 1996).

In this study, the landscape metrics were input as the explanatory variable, and the daily LST mean and LST standard deviation within the community were separately input as the response variable. The RF modelling process consisted of the following steps.

(1) From 2980 community samples, selecting 70 % (i.e., 2086 communities) as training data and 30 % (i.e., 894 communities) as Out of Bag (OOB) data.

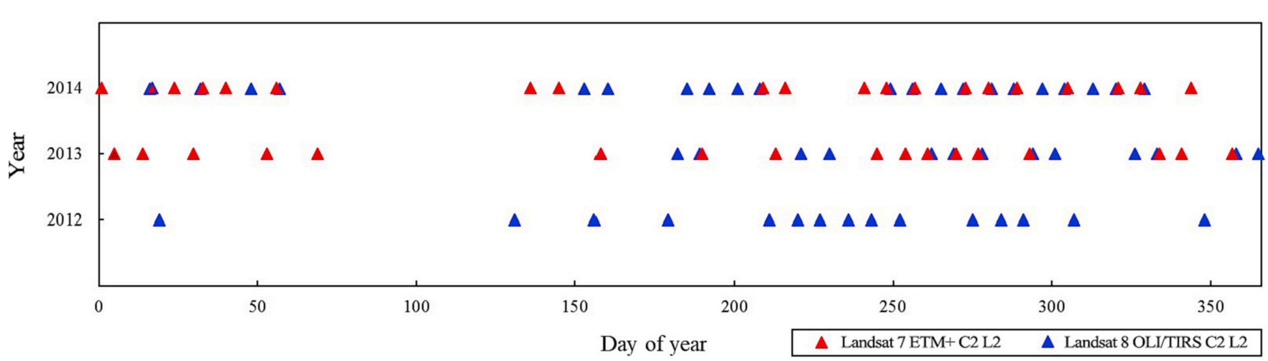

Fig. 7. Temporal distribution of the reserved 86 L2SPs.

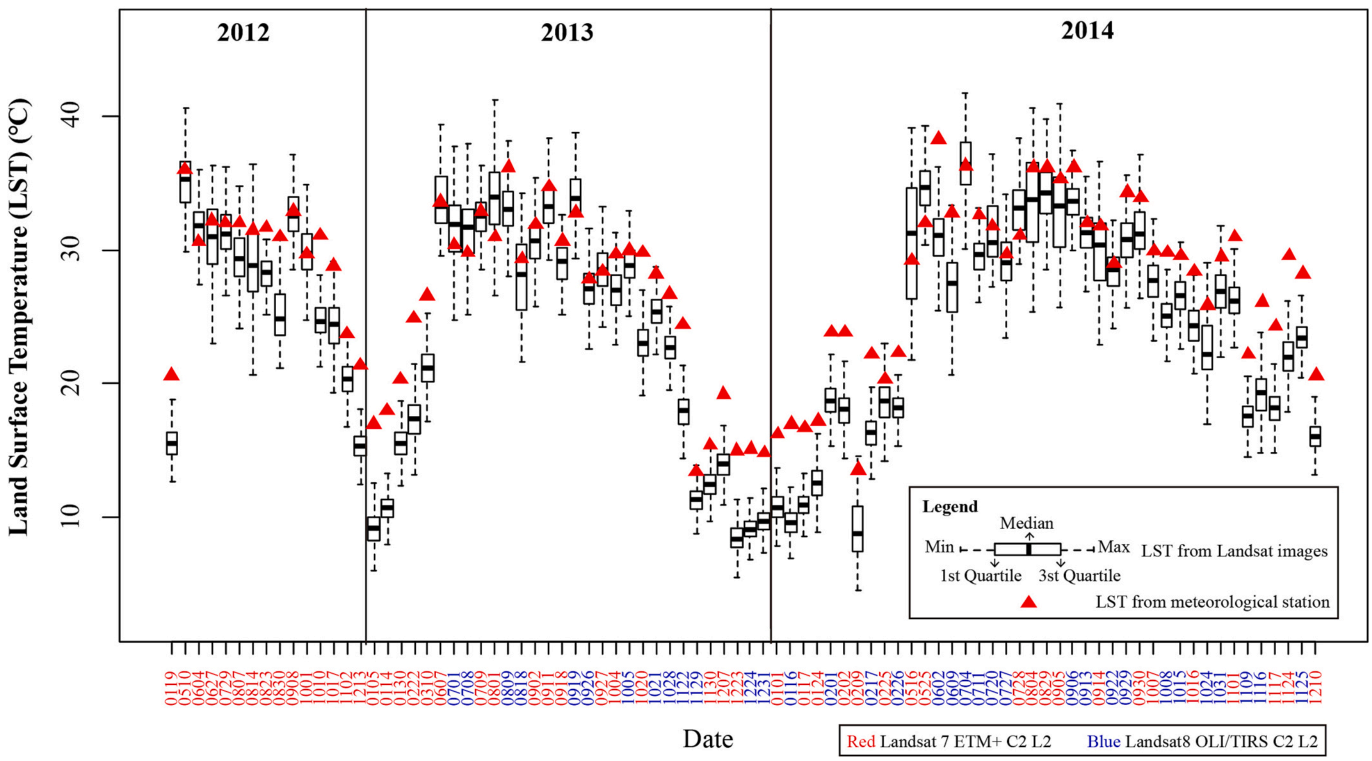

Fig. 8. Accuracy validation of L2SPs based on daily LST averages from meteorological stations (86 days in total).

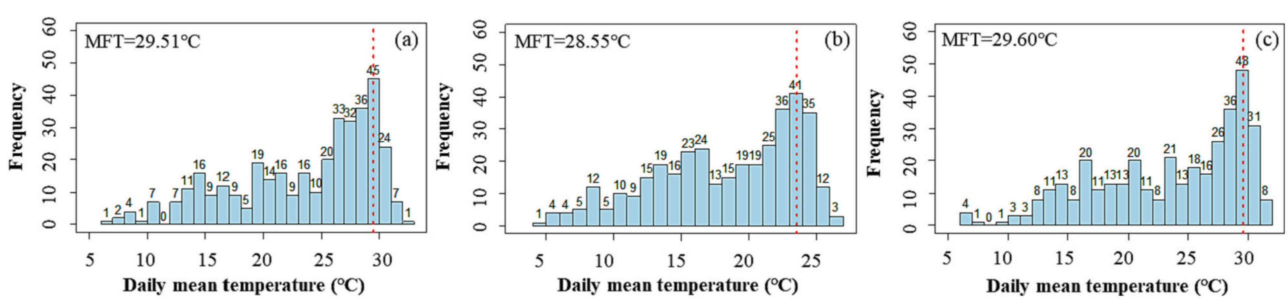

Fig. 9. The annual MFT value during 2012–2014 in Shenzhen. (a): 2012; (b): 2013; (c): 2014.

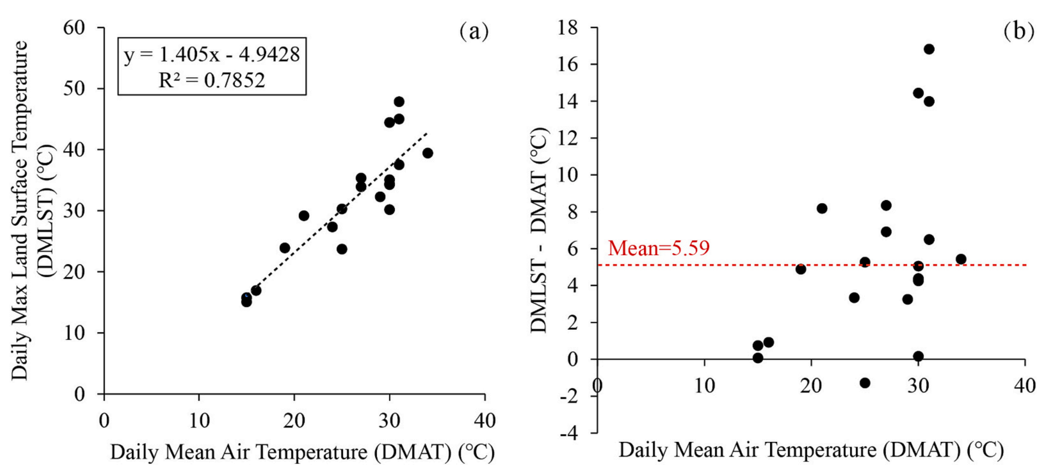

Fig. 10. Validation of the relationship between daily air temperature and daily maximum LST. (a): Linear regression model of daily mean air temperature (DMAT) and daily maximum LST (DMLST); (b): Scatterplot of the difference between DMAT and DMLST with the DMAT.

(2) Based on the Bagging algorithm (Breiman, 2001), generating 2086 regression trees $T_n(x)$ as the samples at the root nodes of the trees.
(3) When each node of the regression tree needs to be split, randomly selecting *mtry* from the 28 community landscape metrics for binary splitting. Here, for each model, this study set the *mtry* for each tree number to 1, 2, ..., 28 (28 is the total number of landscape metrics) for iterative operations, and finally selecting an *mtry* value that minimizes the model's misjudgment rate.
(4) Repeat the process in step (3) until the leaf nodes were reached.
(5) Averaging the prediction results R_n of 2086 regression trees $T_n(x)$ to obtain the final regression result $\overline{R}_n$. The regression equation was as follows.

$$\overline{R}_n = \frac{1}{2086}\sum_{n=1}^{2086} R_n \tag{1}$$

In addition, to ensure the robustness of the results, this study run each model 10 times and took the average as the final result.

(6) Validating the model accuracy based on 894 OOB community sample data. The model error was calculated as follows.

$$MSE^{OOB} = \frac{1}{894}\sum_{n=1}^{894} (\widehat{R}_{n-}R_n) \tag{2}$$

where $\widehat{R}_n$ and R_n are the predicted and observed output, respectively.

In addition to assessing model accuracy, MSE^{OOB}can also be used to measure the importance of each explanatory variable (Breiman, 2002). By randomly replacing the value of a community landscape metric in the training sample, the change in the residuals after the replacement can be calculated. The larger the change, the greater the influence intensity of the landscape feature on the community thermal environment.

Compared with linear regression models and logistic regression models, RF regression models can better solve the problems that this study wants to explore in the following ways: (1) judging the importance of community landscape feature variables to indicate their influence intensity (Hou et al., 2023a); and (2) plotting the dependence curves between the explanatory and response variables to visualize the influence rules of each landscape feature variable on the community LST. Besides, considering the large number of variables selected for this study, the RF model is more advantageous in handling high-dimensional data and is less prone to overfitting.

4. Results

4.1. The influence intensity of community landscape variables on the thermal environment and their temporal variation

Two variables, LST mean and LST standard deviation, were used in this study to describe the thermal environment within the community, and they were separately input into the random forest regression models as response variables. Each model runs 10 times for the robustness of the results. The average interpretability of the LST mean model ranged from 53 % to 80 %, while the average interpretability of the LST standard deviation model ranged from 54 % to 70 % (Fig. S2).

Figs. 11 and 12 presented the ranking of the influence intensity of each landscape metric on the LST mean and LST standard deviation for each of the 86 random forest models, respectively, where the top three landscape metrics were highlighted.

From Fig. 11, the 3D building structure metrics and the 2D landscape composition metrics were the primary variables that affected the community LST means on most days. Specifically, among the 3D building structure metrics (i.e., variables in blue in the first column), average building height (MEAN_HEIGHT), the average shape coefficient of building (MEAN_SC), the average sky view factor of building (MEAN_SVF), the volume ration of building (PLOT_RATIO), and the standard deviation of building height (STD_HEIGHT) were the top three important variables in 65, 29, 18, 17, and 9 days, respectively, while the effect of the orientation variance of building (OV) on the LST mean was always weak. Among the 2D landscape composition metrics (i.e., variables in orange in the first column), the proportion of tree (PLAND_TREE), the proportion of grass (PLAND_GRASS), the proportion of building (PLAND_BUILDING), and the proportion of OIS (PLAND_OIS) had a decisive influence on the LST mean in 42, 21, 8, and 4 days, respectively, while the proportion of soil (PLAND_SOIL), the proportion of water body (PLAND_WATER), and the proportion of road (PLAND_ROAD) variables could barely affect the LST mean due to their low proportion within the community. In contrast, among the 2D landscape structure metrics (i.e., variables in grey in the first column), only the average proximity of building (PROX_MN), the largest patch index of building (LPI), and the landscape shape index of building (LSI) showed pronounced effects on LST means in 8, 7, and 7 days, respectively.

Unlike the results of the community LST mean model, the dominant variables of the community LST standard deviation were almost all 2D landscape structure metrics (Fig. 12). Statistically, the landscape shape index (LSI), the average similarity of building (SIMI_MN), the largest patch index (LPI), the patch density of building (PD), the average proximity of building (PROX_MN), the edge density of building (ED), the area-weighted average perimeter-area ratio of grass (PARA_AM_GRASS), and the splitting index of tree (SPLIT_TREE) influenced the standard deviation of community LST in 83, 82, 63, 6, 5, 1, 1, and 1 days, respectively.

In the time series, the influence intensity rankings of the dominant variables varied less on the daily scale, but obviously on the monthly scale. For example, the importance ranking of the proportion of tree (PLAND_TREE) variable reached its peak in March (Fig. 13 (a)), which was mainly related to the vegetation growth cycle. In general, vegetation grows vigorously during March–August, and its life activity gradually decreases as the weather turns colder. The influence of 2D landscape structure metrics (Fig. 13 (b), (e)) and 3D building structure metrics (Fig. 13 (c), (f)) were more intense in September–March and less intense in May–August, which can be attributed to the change of solar altitude angle. In summer, when the solar altitude angle is large in Shenzhen, buildings have limited shading of solar radiation, while in winter, the 2D and 3D structure metrics of buildings become the dominant factors that affect the LST mean of the community. It should be noted that the LST images used for this study are missing in a large amount in April, so the analysis of this month is deficient.

4.2. The influence rules of community landscape variables on the thermal environment and their temporal variation

According to the findings in Section 4.1, the average building height (MEAN_HEIGHT) and the proportion of tree (PLAND_TREE) were found to be the most important variables influencing the community LST mean. Herein, Figs. 14 and 15 demonstrated the influence rules of these two variables on the LST mean and their temporal variation over 86 days. From Fig. 14, it can be found that in most days, the positive regression coefficient at low MEAN_HEIGHT values implied that increasing the MEAN_HEIGHT value could lead to an elevation of the community LST mean, while as it increased to a threshold, the regression coefficient becomes negative, implying that it would cool the community thermal environment when the building height exceeds a certain value. On average, MEAN_HEIGHT reached its maximum cooling effect when it was around 40-60 m, and this threshold was relatively lower in summer.

When the buildings in the community were low-heighted, the flow of the lower atmosphere will take away part of the heat from the surface, resulting in a low LST (Li et al., 2019), while when the buildings in the community were tall, they could reduce the community LST both by intercepting the solar radiation and casting shadows on the surface (Huang and Wang, 2019). For medium-heighted buildings, they could

	0101	0105	0114	0116	0117	0119	0124	0130	0201	0202	0209	0217	0222	0225	0226	0310	0510	0516	0525	0602	0604	0607	0609	0627	0701	0704	0708	0709	0711
PLAND_OIS	28	4	19	12	21	26	16	10	10	10	11	16	15	28	15	12	10	21	12	11	12	10	21	21	8	28	3	6	20
PLAND_GRASS	19	15	22	18	26	9	17	19	16	12	1	22	14	1	7	4	1	1	2	3	4	2	23	7	12	11	1	15	18
PLAND_TREE	18	7	4	10	18	3	21	7	4	3	3	14	2	21	8	2	11	26	1	4	3	25	2	10	4	1	5	1	24
PLAND_SOIL	26	27	27	28	15	20	28	20	28	27	27	28	27	21	15	28	18	18	12	26	23	14	11	24	27	27	27	14	17
PLAND_BUILDING	10	19	6	16	15	12	19	5	19	5	26	20	13	15	10	9	2	2	4	5	1	22	16	20	1	13	23	22	15
PLAND_WATER	25	25	24	27	23	23	25	27	27	24	28	27	28	27	6	26	23	27	17	27	24	12	27	25	24	23	28	19	5
PLAND_ROAD	15	14	20	14	7	7	20	25	18	19	24	17	23	10	19	23	27	8	25	22	25	1	25	11	23	22	18	3	27
PD	11	6	10	10	8	6	5	26	8	13	5	13	18	26	25	11	28	25	27	8	5	2	15	5	15	18	9	20	10
LPI	6	20	13	7	3	16	7	6	5	13	18	8	8	5	22	8	7	17	24	20	6	20	18	19	26	10	16	11	22
ED	8	5	8	18	11	14	10	15	7	18	21	5	12	13	18	6	22	6	9	10	10	5	3	3	16	7	10	27	4
LSI	4	13	16	2	6	17	9	11	15	21	15	6	5	7	28	19	14	7	20	19	26	7	9	13	28	17	14	23	26
SHAPE_MN	9	24	15	26	25	22	10	20	25	11	7	19	17	8	27	20	24	10	18	9	14	11	24	7	18	19	12	26	28
CIRCLE_MN	12	16	12	23	17	19	18	22	22	20	16	25	26	24	24	25	26	5	10	28	13	27	14	28	17	9	25	24	9
CONTIG_MN	13	10	23	21	24	24	14	28	26	28	19	24	25	18	9	27	20	28	25	21	21	18	10	11	13	20	26	17	2
PROX_MN	21	8	26	9	18	2	12	9	17	7	23	10	24	19	21	12	20	13	19	16	15	26	5	4	4	5	12	10	13
SIMI_MN	5	23	17	8	13	27	15	17	20	17	14	20	9	16	11	21	17	3	28	13	27	16	19	1	10	25	22	9	16
COHESION_MN	16	22	7	13	4	13	8	12	13	25	19	12	19	12	23	14	6	12	15	23	9	17	12	17	9	16	24	12	12
AI	14	8	5	17	14	15	13	23	12	16	22	7	16	11	26	17	15	20	14	25	28	12	19	15	14	26	7	13	8
PARA_AM_GRASS	20	21	25	20	12	21	22	24	21	23	2	18	20	23	3	14	3	4	7	18	20	28	28	26	11	21	6	25	21
SPLIT_GRASS	22	11	28	21	5	18	26	18	23	21	8	11	22	20	14	22	4	18	21	12	19	24	26	22	25	15	4	28	25
PARA_AM_TREE	27	17	18	25	20	10	24	13	9	9	12	23	6	25	11	10	11	15	5	16	16	21	8	6	19	8	17	8	19
SPLIT_TREE	17	26	11	15	22	11	27	8	14	6	9	26	11	17	2	17	18	24	7	13	21	15	6	9	20	12	19	4	23
OV	23	18	21	24	27	25	23	16	24	26	10	15	21	6	17	23	15	9	15	24	17	7	13	27	20	24	21	15	7
MEAN_HEIGHT	1	2	1	1	1	1	1	1	1	1	4	1	1	1	5	1	5	22	3	2	11	6	4	2	3	4	2	2	14
STD_HEIGHT	3	28	2	3	10	28	6	2	11	8	13	9	6	14	13	7	13	14	22	15	8	4	17	14	7	2	20	20	5
PLOT_RATIO	7	3	9	3	9	4	3	4	3	4	6	4	3	3	4	5	8	16	11	7	18	9	21	16	2	14	15	7	11
MEAN_SC	2	1	3	5	2	5	4	3	2	2	25	3	4	4	19	3	9	23	6	6	7	19	7	23	6	6	11	5	1
MEAN_SVF	24	12	14	6	28	8	2	14	6	15	17	2	9	1	1	16	25	11	23	1	2	23	1	17	22	3	8	18	3

	0720	0727	0728	0729	0801	0804	0807	0809	0814	0818	0823	0829	0830	0902	0905	0906	0908	0911	0913	0914	0918	0919	0922	0926	0927	0929	0930	1001	1004
PLAND_OIS	22	3	21	5	18	6	5	13	7	25	8	1	18	11	4	6	24	20	10	1	17	11	27	8	10	11	7	24	15
PLAND_GRASS	8	16	9	21	1	9	6	1	1	25	20	5	12	8	3	4	15	3	16	3	3	8	9	5	8	25	6	18	13
PLAND_TREE	12	2	2	1	7	3	1	7	3	1	2	2	5	14	1	2	4	2	1	17	9	3	19	2	2	1	5	21	2
PLAND_SOIL	20	9	27	25	12	21	8	24	28	21	10	23	20	26	25	23	26	27	24	18	24	18	15	27	22	28	27	25	27
PLAND_BUILDING	24	7	6	7	4	7	3	10	25	15	22	4	21	17	12	7	14	4	12	13	13	15	3	7	6	6	3	9	5
PLAND_WATER	21	21	26	27	19	22	18	28	26	21	12	26	24	24	28	27	19	25	27	15	23	28	14	28	28	26	28	26	28
PLAND_ROAD	10	15	8	26	16	28	24	27	9	19	16	10	27	23	27	28	25	28	14	21	19	19	11	17	24	19	21	12	24
PD	25	14	25	2	14	10	17	19	13	17	1	9	10	10	8	12	5	8	17	8	18	11	20	11	13	12	20	14	10
LPI	3	12	15	4	21	12	22	17	18	25	28	12	25	2	24	17	13	11	11	5	5	8	25	4	11	10	9	3	7
ED	13	22	23	6	6	2	12	9	6	4	7	6	23	14	15	18	11	17	26	27	22	13	24	6	14	3	23	17	6
LSI	14	8	7	15	17	14	26	14	12	3	25	24	9	9	20	21	16	12	2	4	1	16	18	20	17	5	15	10	16
SHAPE_MN	11	4	22	19	27	15	23	23	14	13	11	20	28	20	16	26	12	22	28	22	5	21	5	25	26	23	15	5	21
CIRCLE_MN	28	11	28	23	9	26	14	26	4	2	24	14	14	21	17	25	27	6	13	25	7	27	21	26	21	18	17	28	25
CONTIG_MN	5	12	13	16	15	5	21	22	15	27	4	22	8	19	25	23	22	21	21	10	20	25	26	21	20	20	18	23	26
PROX_MN	27	25	14	18	10	11	20	20	10	21	4	28	2	3	6	3	18	13	23	20	10	26	4	22	3	14	8	3	18
SIMI_MN	9	26	16	17	24	1	10	17	23	7	27	15	1	18	6	13	6	13	4	8	16	23	13	18	7	22	14	11	20
COHESION_MN	7	10	12	12	26	13	18	11	16	27	6	18	22	4	11	16	20	19	7	13	27	17	28	15	16	15	13	13	11
AI	23	23	19	10	24	4	28	4	20	5	17	25	15	7	14	19	17	22	8	7	7	14	15	14	9	9	11	7	17
PARA_AM_GRASS	19	28	17	22	22	26	11	8	8	14	18	26	7	28	13	14	1	26	15	12	12	24	10	19	26	27	24	22	22
SPLIT_GRASS	16	27	20	20	20	25	25	12	5	23	23	21	3	24	22	22	21	15	19	24	11	22	17	23	25	24	25	16	19
PARA_AM_TREE	17	17	11	3	10	16	15	15	22	10	20	17	19	27	9	11	10	24	18	27	25	6	23	16	12	21	12	20	8
SPLIT_TREE	18	18	10	8	5	17	13	16	11	12	15	19	17	22	18	15	23	18	19	25	28	10	6	13	15	13	19	27	9
OV	26	18	24	28	28	19	27	25	17	9	19	16	26	6	22	20	8	15	25	19	14	20	21	24	22	17	26	18	23
MEAN_HEIGHT	3	5	1	12	2	24	7	2	21	11	13	3	3	1	2	1	3	1	3	11	4	1	1	1	1	2	1	1	1
STD_HEIGHT	14	6	18	14	8	8	16	21	18	6	9	13	15	5	21	8	2	5	6	16	26	5	12	12	18	16	22	15	14
PLOT_RATIO	1	1	5	23	13	18	9	5	24	18	26	11	11	12	10	10	7	10	9	23	14	4	8	10	4	7	10	6	4
MEAN_SC	2	20	3	11	23	20	4	6	26	16	3	7	13	16	5	5	9	9	5	6	2	2	7	3	5	4	4	2	3
MEAN_SVF	6	24	4	9	3	23	2	3	2	8	14	8	6	13	19	9	28	6	22	2	20	7	2	8	19	7	2	7	12

	1005	1007	1008	1010	1015	1016	1017	1020	1021	1024	1028	1031	1101	1102	1109	1116	1117	1122	1124	1125	1129	1130	1207	1210	1213	1223	1224	1231	
PLAND_OIS	9	9	6	10	7	8	12	10	8	6	12	4	16	21	19	5	11	4	15	16	6	21	12	16	14	7	18	26	
PLAND_GRASS	13	3	8	13	1	19	1	4	12	9	2	1	15	7	9	6	24	16	8	22	2	12	9	11	15	18	28	25	
PLAND_TREE	2	2	2	5	10	2	3	2	2	1	5	3	3	4	22	3	6	9	22	2	7	3	26	1	25	4	14	21	
PLAND_SOIL	23	27	22	26	27	17	14	27	28	24	27	27	14	27	23	27	25	28	23	27	27	26	28	2	27	26	24	28	
PLAND_BUILDING	5	12	9	6	8	19	5	5	7	11	9	16	6	22	1	22	8	14	16	15	18	10	21	4	10	23	14	22	
PLAND_WATER	28	28	27	27	28	24	25	28	27	25	28	28	22	28	28	28	23	25	27	28	28	27	27	5	28	28	27	27	
PLAND_ROAD	19	25	25	23	24	15	26	22	18	5	21	20	19	26	8	23	12	19	11	21	24	15	19	19	13	26	21	13	
PD	15	23	13	21	15	22	28	18	14	8	17	8	11	10	7	12	19	21	14	7	15	5	4	14	6	12	19	8	
LPI	12	7	15	8	4	7	16	7	14	15	3	8	7	5	4	8	12	12	18	5	4	8	6	12	17	3	2	7	
ED	14	19	14	14	9	21	4	3	14	14	4	13	12	11	2	15	7	6	8	6	14	2	8	9	11	15	17	10	
LSI	17	10	18	9	13	12	17	16	17	4	8	12	17	9	16	7	20	17	7	13	9	22	6	27	9	6	6	3	
SHAPE_MN	25	22	28	22	23	28	20	17	24	18	23	23	25	14	25	20	17	11	20	20	21	25	13	26	7	17	13	16	
CIRCLE_MN	23	18	21	17	25	9	15	21	22	23	26	25	10	15	5	19	18	12	25	26	22	23	25	23	7	13	22	17	
CONTIG_MN	21	26	26	27	26	15	24	26	25	19	25	26	21	25	17	24	14	10	18	12	26	11	15	25	24	19	23	14	
PROX_MN	7	13	12	4	20	5	18	12	9	7	18	22	2	20	24	25	2	8	5	17	16	24	17	7	17	22	11	14	
SIMI_MN	16	15	16	16	21	27	21	19	19	20	19	17	24	16	3	17	20	26	13	10	23	19	5	22	3	21	16	11	
COHESION_MN	18	11	17	12	17	14	22	13	16	27	13	15	18	8	13	18	3	18	24	8	8	20	18	20	20	8	8	12	
AI	20	8	19	7	14	25	2	14	20	22	10	14	20	13	10	13	4	15	17	19	19	16	11	23	4	11	20	9	
PARA_AM_GRASS	26	14	20	24	4	18	7	25	23	10	22	10	26	17	11	14	27	24	21	24	13	7	20	15	25	25	26	24	
SPLIT_GRASS	22	17	24	25	3	23	9	20	21	13	20	11	13	23	20	21	22	22	10	24	11	14	23	9	21	20	25	23	
PARA_AM_TREE	8	19	4	18	18	11	27	9	4	21	15	19	8	19	27	16	28	23	28	18	20	13	24	12	22	10	12	20	
SPLIT_TREE	10	21	4	19	16	10	23	11	6	17	11	21	9	17	26	10	26	20	26	11	17	9	22	8	22	9	5	18	
OV	27	24	23	20	22	25	19	24	26	28	24	24	27	24	12	26	9	7	12	24	25	27	10	28	19	24	10	19	
MEAN_HEIGHT	1	1	1	1	2	1	11	1	1	12	1	2	1	1	15	1	1	1	1	1	1	1	1	3	1	1	1	1	
STD_HEIGHT	11	15	11	15	19	6	10	15	10	26	13	18	28	6	14	9	15	3	2	14	10	18	3	6	15	14	4	5	
PLOT_RATIO	4	6	7	3	6	3	8	6	5	3	5	6	5	2	21	4	5	5	6	4	3	6	2	18	2	5	3	4	
MEAN_SC	3	4	3	2	11	4	6	8	3	16	7	4	4	3	18	2	15	2	3	3	5	4	14	21	5	1	7	2	
MEAN_SVF	6	5	10	11	12	13	12	22	11	2	16	7	23	12	6	11	10	27	4	9	12	17	16	17	12	15	9	6	

Fig. 11. Daily rankings of the influence intensity of landscape metrics on LST mean in the random forest models (86 days in total).

	0101	0105	0114	0116	0117	0119	0124	0130	0201	0202	0209	0217	0222	0225	0226	0310	0510	0516	0525	0602	0604	0607	0609	0627	0701	0704	0708	0709	0711
PLAND_OIS	14	19	21	19	22	18	19	14	22	22	21	21	16	22	5	18	28	18	24	12	22	6	11	27	26	14	23	27	28
PLAND_GRASS	25	17	16	10	13	15	11	16	21	16	18	22	19	12	24	17	16	21	8	4	17	20	23	7	9	20	16	7	18
PLAND_TREE	21	13	18	21	16	20	18	23	27	27	13	23	23	16	18	19	26	8	18	18	27	19	5	12	23	10	9	22	25
PLAND_SOIL	27	25	22	25	5	23	27	27	11	17	24	17	27	28	10	25	20	26	14	23	23	13	20	15	20	24	25	12	26
PLAND_BUILDING	23	21	25	16	20	24	16	15	19	18	19	18	12	11	28	14	27	6	23	25	20	5	7	17	22	13	11	15	14
PLAND_WATER	26	26	27	28	26	28	28	24	28	26	28	28	28	27	12	28	25	22	16	27	26	15	24	18	25	25	28	14	24
PLAND_ROAD	9	28	11	23	27	6	20	22	14	24	27	12	21	14	6	27	19	7	15	13	12	8	12	28	11	17	12	24	10
PD	13	6	4	4	11	8	4	10	5	7	4	5	4	9	15	7	5	4	11	7	14	21	8	2	4	12	5	23	7
LPI	4	3	5	3	3	5	3	4	3	5	3	3	3	3	7	4	3	3	21	3	2	2	2	5	2	3	3	3	4
ED	8	11	10	8	8	13	9	7	9	10	7	9	7	17	16	8	10	14	4	15	5	24	9	18	5	8	8	20	8
LSI	2	2	3	2	2	2	2	2	2	2	1	2	2	2	1	2	2	2	2	1	1	1	1	4	1	1	2	1	3
SHAPE_MN	27	12	23	22	23	26	25	20	24	25	16	25	13	18	27	16	10	16	28	24	16	18	25	13	21	28	27	10	9
CIRCLE_MN	15	22	25	24	25	12	23	17	25	23	20	27	25	21	22	26	12	26	8	28	15	25	14	20	27	18	26	28	27
CONTIG_MN	20	16	15	15	28	27	14	13	18	9	10	20	17	19	14	21	13	25	10	20	19	17	22	26	17	27	20	26	16
PROX_MN	10	4	8	5	14	4	8	9	4	4	6	4	5	6	4	3	4	12	3	7	18	10	19	3	8	4	4	5	5
SIMI_MN	1	1	1	1	1	1	1	1	1	1	2	1	1	1	2	1	1	1	1	2	3	3	3	1	3	2	1	2	1
COHESION_MN	12	7	17	17	19	22	15	18	15	12	8	11	15	20	26	11	22	9	22	22	8	16	18	22	12	16	24	17	20
AI	19	27	12	12	18	16	13	11	10	11	16	10	10	15	20	13	24	23	26	16	13	12	27	22	23	5	13	13	23
PARA_AM_GRASS	11	23	9	14	7	16	22	19	20	20	26	19	20	26	12	20	18	24	20	10	25	10	17	14	16	15	15	8	19
SPLIT_GRASS	24	20	14	11	15	11	21	21	16	28	11	13	18	8	18	15	7	11	27	20	9	27	12	9	19	20	7	4	22
PARA_AM_TREE	22	24	24	26	24	21	24	28	26	21	25	25	26	25	9	21	15	15	19	17	28	26	28	10	13	22	19	19	17
SPLIT_TREE	18	10	28	20	17	9	10	26	12	19	15	15	22	24	21	23	14	13	13	9	23	28	14	8	15	23	18	9	15
OV	5	15	6	6	12	3	5	6	6	6	5	5	9	5	3	5	23	5	16	5	6	22	6	11	7	11	6	6	2
MEAN_HEIGHT	7	7	7	6	6	14	7	3	8	8	12	8	8	7	23	5	6	19	6	19	20	14	21	24	18	6	22	16	6
STD_HEIGHT	3	5	2	9	4	7	6	5	7	3	22	7	6	4	10	9	17	17	7	6	4	9	4	5	10	9	10	17	12
PLOT_RATIO	6	14	18	13	10	10	11	8	13	15	9	16	14	13	24	12	9	28	12	11	10	7	10	25	14	19	21	21	21
MEAN_SC	16	9	13	18	9	19	17	12	17	13	14	14	11	10	17	10	21	20	25	26	7	22	16	16	27	7	17	10	11
MEAN_SVF	17	18	20	27	21	24	26	25	23	14	23	25	23	23	8	24	8	10	5	14	11	4	26	21	6	26	14	25	13

	0720	0727	0728	0729	0801	0804	0807	0809	0814	0818	0823	0829	0830	0902	0905	0906	0908	0911	0913	0914	0918	0919	0922	0926	0927	0929	0930	1001	1004
PLAND_OIS	15	28	20	12	14	20	21	20	22	17	19	12	22	20	22	23	10	17	10	17	19	25	12	12	19	11	26	19	23
PLAND_GRASS	2	12	27	5	11	16	26	16	5	7	5	15	5	27	15	5	3	4	8	15	15	10	4	16	5	12	14	22	8
PLAND_TREE	28	11	23	16	8	15	15	17	28	6	28	24	9	13	18	20	9	11	19	10	13	21	24	22	14	9	10	11	12
PLAND_SOIL	24	16	7	22	24	12	20	19	14	24	16	28	7	26	24	25	21	24	15	1	10	13	21	27	25	25	16	27	19
PLAND_BUILDING	22	10	8	15	11	23	19	14	19	19	26	19	20	10	14	18	18	12	21	9	28	16	13	12	8	19	23	7	11
PLAND_WATER	23	23	26	24	25	14	23	28	24	22	14	23	25	19	26	28	24	27	25	25	16	27	26	28	28	28	25	25	28
PLAND_ROAD	21	12	12	4	17	13	7	26	21	28	9	17	26	24	28	26	26	25	26	6	26	24	23	10	23	18	21	23	22
PD	8	20	9	7	5	18	11	5	4	10	3	9	4	4	4	8	11	10	6	3	4	8	9	4	3	5	6	6	4
LPI	7	3	3	3	2	2	6	3	3	3	4	3	3	3	3	3	2	3	3	5	3	3	8	3	6	3	5	2	3
ED	17	19	4	9	16	6	4	6	13	27	10	16	10	16	7	6	4	13	17	16	11	13	16	6	7	4	15	5	6
LSI	1	2	2	2	3	2	2	2	2	1	1	1	1	2	2	1	6	2	1	4	2	1	1	1	2	2	1	3	2
SHAPE_MN	14	27	25	20	21	17	28	10	17	25	12	14	15	11	20	22	12	16	22	18	18	26	17	26	22	26	9	28	13
CIRCLE_MN	25	26	10	25	18	28	24	27	10	25	26	18	27	28	26	27	16	23	28	14	25	28	25	25	13	27	27	21	24
CONTIG_MN	20	22	18	27	27	9	15	25	26	21	25	25	14	18	12	20	15	18	20	19	14	23	15	20	24	16	11	16	27
PROX_MN	9	5	6	10	7	5	9	7	9	23	8	5	6	5	5	7	23	6	4	23	8	6	3	8	12	10	3	4	5
SIMI_MN	3	1	1	1	1	1	1	1	1	2	2	2	2	1	1	2	7	1	2	8	1	2	5	2	1	1	2	1	1
COHESION_MN	16	25	12	17	10	27	27	11	15	8	22	22	28	12	21	17	14	26	9	21	20	17	28	11	26	21	8	18	14
AI	19	9	18	21	20	10	25	13	23	11	11	8	7	15	13	13	20	7	12	22	21	11	18	15	20	20	20	17	17
PARA_AM_GRASS	6	14	21	28	23	21	8	17	11	4	6	7	18	25	18	10	22	8	11	2	11	5	11	17	11	22	17	13	20
SPLIT_GRASS	10	21	28	19	6	11	14	9	7	14	7	21	17	22	17	24	27	22	14	24	8	22	14	18	21	13	19	9	16
PARA_AM_TREE	27	15	21	23	13	23	21	22	8	20	23	26	24	14	25	19	19	21	16	28	27	19	20	21	27	24	24	20	25
SPLIT_TREE	26	7	15	14	22	26	10	12	16	9	19	11	12	21	16	13	28	20	23	26	23	9	22	14	17	7	22	10	18
OV	4	4	16	6	26	19	17	4	12	18	15	4	21	6	6	4	25	5	7	13	5	4	2	7	4	8	4	12	9
MEAN_HEIGHT	12	8	17	8	15	22	18	15	20	5	21	10	11	8	9	16	12	14	24	27	6	15	19	9	15	6	18	15	7
STD_HEIGHT	11	6	5	11	19	4	3	8	6	16	18	6	19	17	8	12	1	9	4	7	17	7	7	5	9	14	7	8	10
PLOT_RATIO	18	24	10	18	9	8	13	23	25	13	13	13	13	22	10	9	8	15	27	19	24	13	10	23	10	23	13	23	21
MEAN_SC	13	17	14	13	4	6	12	23	26	15	17	19	23	7	11	15	17	19	18	11	8	18	27	24	18	16	12	14	15
MEAN_SVF	5	17	24	26	28	25	5	21	18	12	24	26	16	9	23	11	5	28	13	12	22	20	6	19	16	15	28	26	25

	1005	1007	1008	1010	1015	1016	1017	1020	1021	1024	1028	1031	1101	1102	1109	1116	1117	1122	1124	1125	1129	1130	1207	1210	1213	1223	1224	1231
PLAND_OIS	22	18	11	23	25	8	23	19	16	7	25	20	28	16	15	22	23	25	15	24	21	18	14	27	19	13	14	22
PLAND_GRASS	8	26	6	26	14	10	27	12	7	20	17	14	10	20	12	13	13	11	27	12	10	11	21	13	14	25	11	20
PLAND_TREE	20	11	19	16	17	26	20	14	12	9	20	22	22	23	20	16	19	21	25	17	19	25	18	23	13	22	15	23
PLAND_SOIL	16	27	25	6	12	7	22	27	17	17	12	17	12	27	27	18	10	12	13	18	15	17	24	18	23	20	22	18
PLAND_BUILDING	17	16	16	15	11	21	12	18	18	8	15	18	21	9	16	11	17	17	14	22	13	27	16	24	23	12	24	15
PLAND_WATER	28	28	28	28	28	20	21	28	28	21	28	28	20	28	28	28	26	27	21	28	28	26	28	16	27	27	28	28
PLAND_ROAD	27	21	22	25	26	22	15	14	20	14	26	23	17	12	22	23	22	16	23	20	15	15	19	12	28	16	23	19
PD	7	6	8	4	5	9	4	4	9	13	5	4	3	4	6	4	4	8	6	8	4	7	5	2	5	5	8	7
LPI	3	3	3	3	3	3	3	3	3	1	3	3	4	3	3	3	9	4	4	3	3	3	3	9	4	3	3	3
ED	10	5	9	8	7	10	6	7	8	15	7	6	6	7	10	7	5	6	8	4	8	8	6	8	3	6	4	8
LSI	1	2	1	1	2	2	2	2	1	2	1	1	2	2	1	2	2	1	2	1	2	2	2	3	2	2	2	2
SHAPE_MN	18	12	22	20	24	28	10	21	27	27	23	16	7	17	14	24	21	24	23	23	25	28	19	19	12	26	27	25
CIRCLE_MN	23	22	27	22	27	15	25	26	24	18	27	25	5	25	18	27	8	19	28	27	27	21	22	10	21	15	26	27
CONTIG_MN	24	20	15	18	22	17	7	22	23	23	19	24	24	24	22	19	28	28	18	21	17	22	26	28	22	24	20	21
PROX_MN	6	7	5	7	4	4	9	5	6	6	4	5	9	5	4	5	6	10	5	4	5	9	6	26	11	7	9	4
SIMI_MN	2	1	2	2	1	1	1	1	2	4	1	2	1	1	2	1	1	2	1	2	1	1	1	1	1	1	1	1
COHESION_MN	21	14	21	23	13	24	17	16	26	16	13	19	14	14	17	15	16	19	11	13	15	19	15	20	17	10	17	13
AI	12	12	13	12	15	25	5	11	14	12	11	13	15	10	9	12	20	15	12	11	10	20	13	5	7	11	13	12
PARA_AM_GRASS	9	19	10	10	16	6	25	23	10	24	16	21	23	18	8	14	12	13	15	9	19	6	17	15	6	21	16	17
SPLIT_GRASS	19	17	24	13	10	23	19	19	21	22	10	10	24	13	24	9	18	22	21	16	12	16	11	14	18	19	19	14
PARA_AM_TREE	26	24	26	19	23	19	28	25	25	5	24	27	18	26	21	25	27	23	17	25	26	12	25	6	25	23	25	24
SPLIT_TREE	11	9	18	9	18	18	23	17	22	3	14	11	19	20	26	21	24	19	19	26	18	13	23	4	20	13	18	16
OV	4	4	7	21	6	14	13	8	4	10	6	9	8	11	7	8	3	14	3	6	7	5	9	25	10	9	6	9
MEAN_HEIGHT	15	9	19	14	9	12	8	6	13	19	9	7	16	8	11	10	7	3	7	10	9	10	4	7	9	8	7	5
STD_HEIGHT	5	8	4	5	8	16	18	9	5	26	8	12	13	5	5	6	11	5	10	7	6	4	8	17	8	4	5	6
PLOT_RATIO	14	15	14	11	21	13	14	13	11	11	22	26	11	14	13	20	14	7	20	14	23	24	10	11	15	17	10	10
MEAN_SC	24	25	16	17	19	5	16	10	19	24	18	15	27	19	19	17	15	9	9	19	24	14	12	22	16	18	12	11
MEAN_SVF	13	23	12	27	20	27	11	24	15	28	21	8	26	22	25	26	25	26	26	15	21	23	27	21	26	28	21	26

Fig. 12. Daily rankings of the influence intensity of landscape metrics on LST standard deviation in the random forest models (86 days in total).

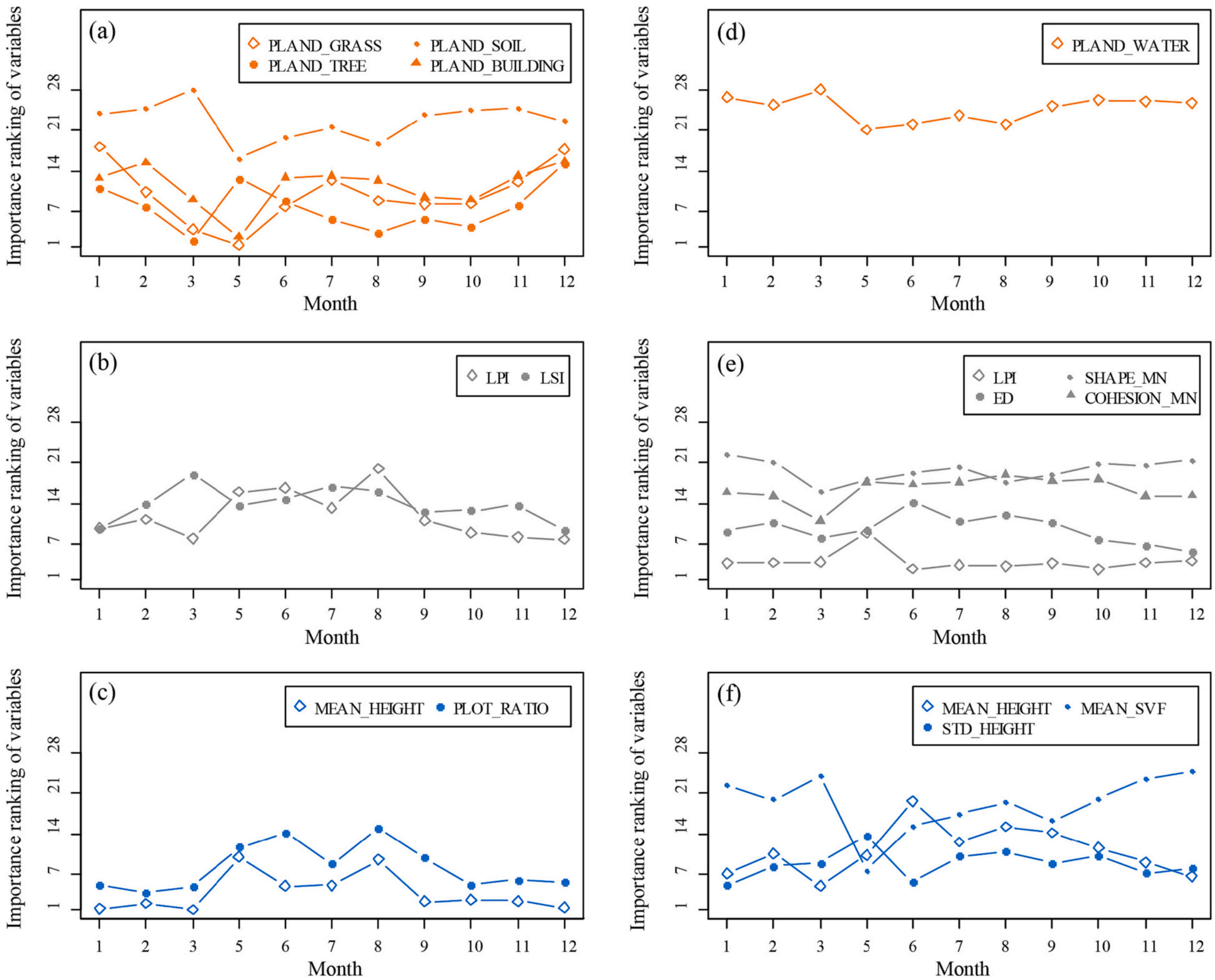

Fig. 13. Monthly rankings of the influence intensity of landscape metrics on LST mean (Left column) and LST standard deviation (Right column) in the random forest models (11 months in total). (a), (d): 2D landscape composition metrics; (b), (e): 2D landscape structure metrics; (c), (f): 3D building structure metrics.

not only hinder the air flow, but also did not provide strong shading, thus causing an increase in LST. Yu et al. (2020) reached similar conclusions by exploring the effect of building height on the thermal environment at a local scale.

In contrast, the regression coefficients of the proportion of tree (PLAND_TREE) in the 86 random forest models were almost all negative (Fig. 15). It gradually decreased as the PLAND_TREE values increased, and finally leveled off. This signified that the increase of tree cover could effectively reduce the mean value of community LST, but the cooling effect of trees would no longer enhance beyond a certain threshold. It was observed that, although there were inter-day variations, in most cases the tree cover could guarantee a significant cooling effect at the community scale when it reached the 20 % threshold. In particular, on the daily scale, the curves of some models (e.g., 0209, 0801, 0814, 0818, 1210) indicated that the increase in tree cover would raise the average community LST, which may be due to some specific meteorological conditions such as low air humidity, since the warming effect of vegetation has been reported in many arid climate zone cities (Yu et al., 2018; Liu et al., 2021a).

In addition to PLAND_TREE and MEAN_HEIGHT, the influence rules of other relatively important landscape metrics on the community thermal environment were as follows: (1) In Fig. S3, the increase of the proportion of grass (PLAND_GRASS) was often accompanied by the decrease in the mean LST (i.e., y-axis values <0). Similar to PLAND_TREE, a strong cooling effect can be achieved when PLAND_GRASS reached 20 % on most days. However, the complexity and inter-day variability of its curve was much higher than that of PLAND_TREE due to its relationship with the LST mean was often disturbed by other dominant variables; (2) In Fig. S4, as the average shape coefficient of building (MEAN_SC) increased from 0 to 2, its regression coefficient increased rapidly in a linear fashion and turned from negative to positive. This indicated that when the MEAN_SC value is low, it was beneficial to reduce the LST mean, while when it was high (especially after it exceeded 2), it was necessary to consider decreasing it to maintain a low community LST; (3) In Fig. S5, the influence rule curve of the average sky view factor of building (MEAN_SVF) presented two opposite shape characteristics of descending and ascending in 86 days. To investigate the reason, we extracted the x-value corresponding to the smallest y-value (i.e., the MEAN_SVF threshold with the strongest cooling effect) from each of the 86 curves for correlation analysis with daily meteorological data (Fig. S6). The results showed that air pressure was the main meteorological factor affecting this threshold: on days with higher air pressure, a larger MEAN_SVF led to a stronger cooling effect, and vice versa, a smaller MEAN_SVF was more conductive for cooling; (4) In Fig. S7, the daily influence rule curves of the volume ratio of building (PLOT_RATIO) were relatively consistent during the 86 days. In general, communities with higher PLOT_RATIO values tended to have more intensive building cooling.

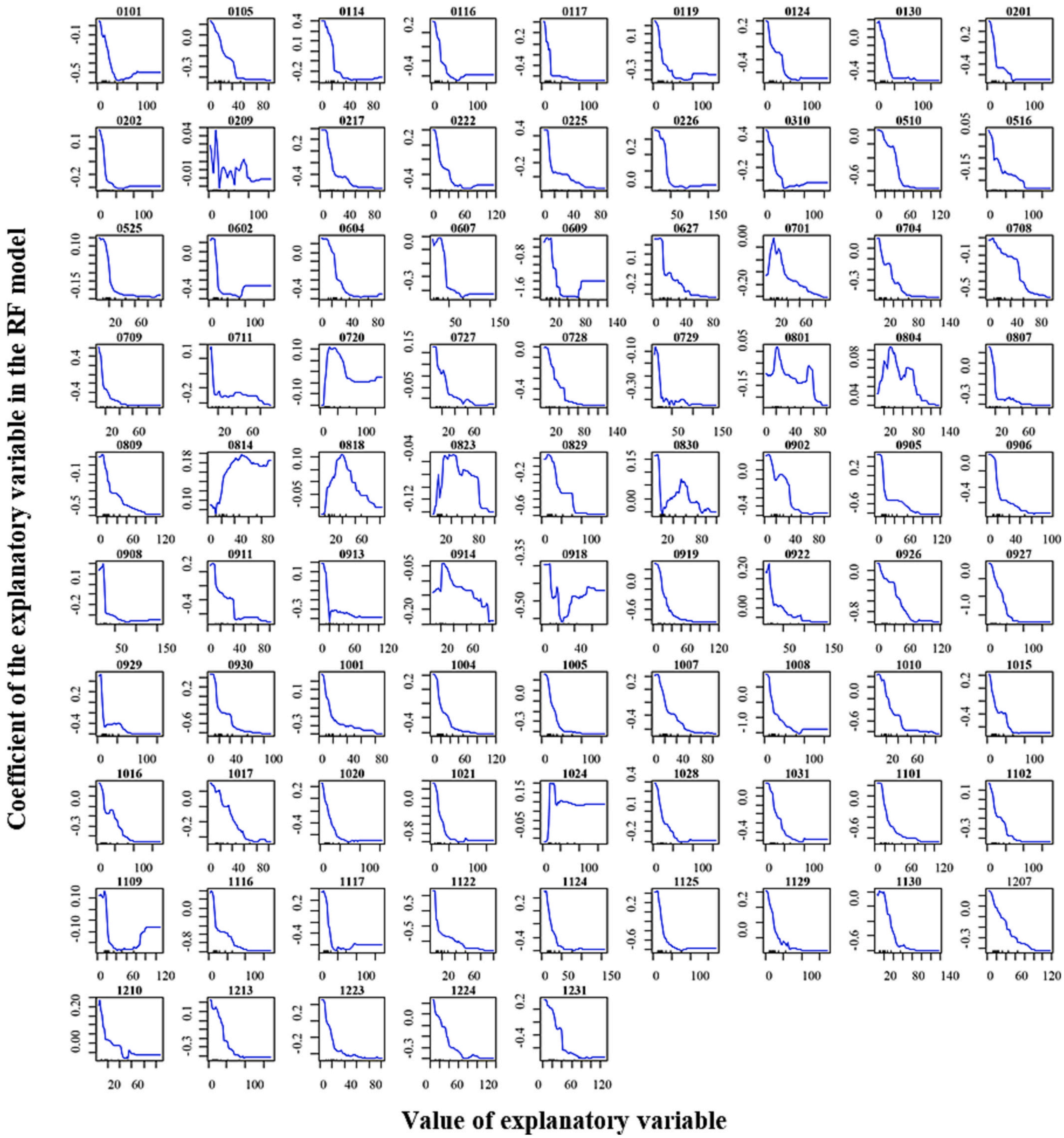

Fig. 14. Influence rules of the landscape metrics on LST mean based on the dependence curves of random forest model, taking the average building height (MEAN_HEIGHT) variable as an example (the number above each chart is the date corresponding to the model).

4.3. Analysis of landscape configuration for maintaining a livable community thermal environment

To analyze what kind of the landscape configuration was conductive to maintaining a livable community thermal environment, the top 10 % communities whose average LST was closest to the LST threshold for thermal livability in Shenzhen (i.e., 35 °C) were extracted (hereafter referred to as "thermally livable communities"), and their landscape metrics were clustered on a daily scale. Fig. 16 displayed the clustering results of six landscape metrics that played a dominant role in affecting the mean LST of the communities.

On most days, except for the average sky view factor of building (MEAN_SVF), the values of other five metrics of thermally livable communities were notably higher than the overall mean value of all communities. Among them, the proportion of grass (PLAND_GRASS) and the proportion of tree (PLAND_TREE) were particularly prominent during June–October, while the average building height (MEAN_-HEIGHT), the volume ratio of building (PLOT_RATIO) and the average

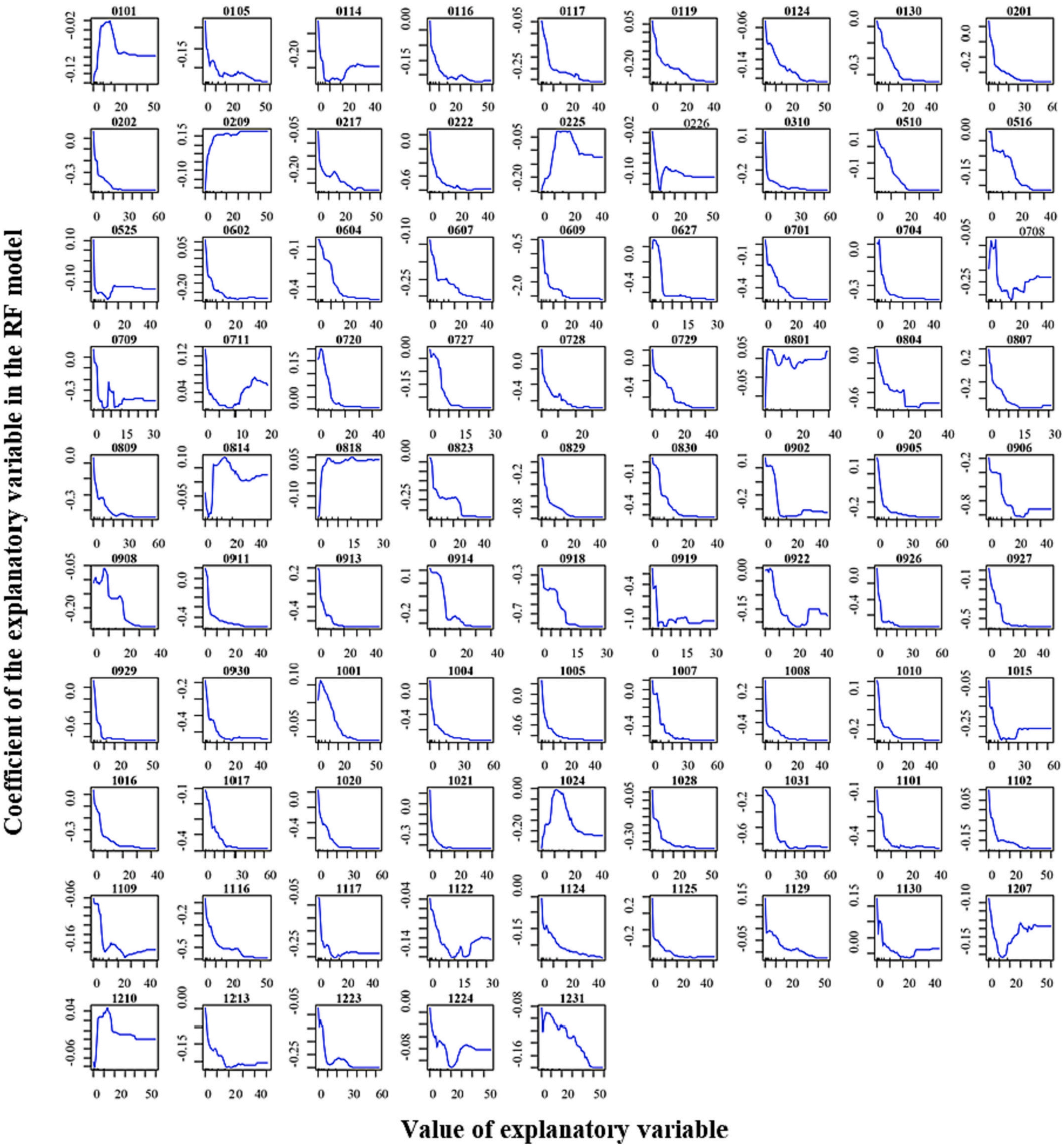

Fig. 15. Influence rules of the landscape metrics on LST mean based on the dependence curves of random forest model, taking the proportion of tree (PLAND_TREE) variable as an example (the number above each chart is the date corresponding to the model).

shape coefficient of building (MEAN_SC) were higher than the overall mean values mainly between July–September, March–September and May–September. This suggested that high grass and tree cover, high building heights and volume ratios, and complex building morphologies were beneficial to maintaining a livable community thermal environment during the summer days. There is no doubt that trees and grasses have a strong cooling effect on the thermal environment in summer, and this has been agreed upon in many studies (Wang et al., 2019; Yang et al., 2021; Liu et al., 2021a,b). For buildings, high average building heights and complex building morphologies are effective in blocking direct sunlight and providing more shade in summer (Li et al., 2020; Li et al., 2021).

In contrast, communities with low PLAND_TREE had a higher thermal livability in the winter days. This is largely due to that both photosynthesis and transpiration of trees slow down in winter, making it difficult for heat to escape. Moreover, trees in a community can prevent surface heat flow caused by cold winds to some extent, allowing the local surface climate to be decoupled from the general climate, thus

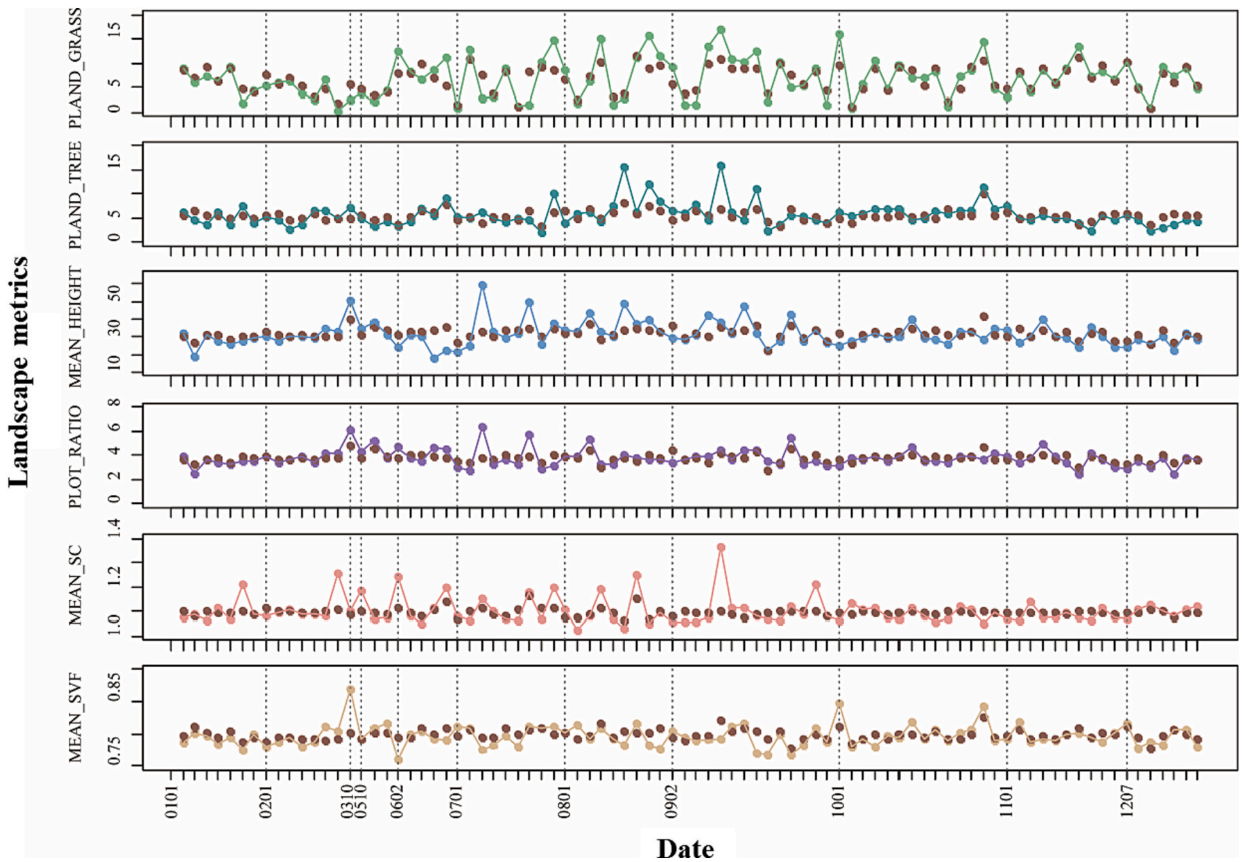

Fig. 16. The average landscape metrics of thermally livable communities (folded lines) and overall communities (scattered points) on a daily scale, taking the six dominant factors affecting the community LST mean as an example.

creating a microclimate refuge (Dobrowski, 2011; Zhou et al., 2017).

Moreover, no matter in summer or winter, the MEAN_SVF of thermally livable communities was generally lower than the overall mean values. This implied that the dense building morphology in 3D space favored the maintenance of thermally livable environments in either warm or cold weathers. The reason, as mentioned above, is that these communities have formed a relatively independent local microclimate environment due to avoiding strong heat flow (Yu et al., 2021). It should be emphasized that this tendency was not absolute or invariant owing to varied meteorological conditions and complex synergistic effects between landscapes.

5. Discussion

5.1. Relationship between landscape and thermal environment at different scales

Current researches have reached some consensus on the influence of the 2D composition of the landscape on the thermal environment at the city scale. It is generally agreed that high-coverage vegetation and water bodies were the essential “cooling sources” in cities, while buildings and other impervious surfaces were the primary “heating sources” (Cao et al., 2010; Zhou et al., 2017). This finding was also confirmed in this community-scale study. Notwithstanding, at the community scale, the influence intensity of different landscapes on the thermal environment differed from that at the city scale. Numerous studies have reported that building occupancy was the overarching factors in determining the overall thermal environment at the city scale (Guo et al., 2020; Yuan et al., 2021; Hou et al., 2023b), whereas this study found that for communities, tree cover was a more critical factor for average LST values. In addition, due to the limited coverage of water body, its influence on thermal environment was almost negligible at the community scale, which was also contrary to the findings at the city scale.

This inconsistency is chiefly owing to the differences in the landscape and human activities across different scales. At the city scale, buildings are usually the most dominant and densely distributed landscape, while trees have a limited share and are often planted as the secondary landscapes interspersed between buildings. In the areas with high building coverage, especially in commercial and industrial functional zones, there is usually high intensity of human activity in daytime, resulting in considerable anthropogenic heat emissions (Tong et al., 2020). By contrast, at the community scale, the population density is lower during the daytime, and the heat emission from living activities is far less than that from commercial and industrial activities. More importantly, the cooling intensity of trees on their surrounding surface thermal environment would be amplified at a smaller community scale according to the “island theory” (Ziter et al., 2019). Based on previous studies, about 40 % tree cover can dominantly influence the LST at the city scale (Liu et al., 2021a,b), while this study reported that only 20 % tree cover can prominently cool down the land surface at the community scale. Likewise, it can be concluded that there is a difference in the influence on the thermal environment between large water bodies (e.g., lakes, rivers, etc.) discussed at the city scale and fragmented water bodies (e.g., fountains, swimming pools, etc.) within the community.

This scale effect was also witnessed in the results of the 3D landscape structure metrics. The findings of existing studies on the relationship between building height and LST in cities were contradictory. For example, Berger et al. (2017) revealed that taller buildings in cities were prone to lead to urban heat island effect, while Huang and Wang (2019) and Zheng et al. (2019) concluded that an increase in building height is beneficial in mitigating urban heat. In this study, it was found that at the community scale, as the average building height increased, LST showed a varied curve that first ascended and then descended, and when it was around 40-60 m, its cooling intensity reached the maximum. It can be seen the analysis at the micro-community scale can better expose the complex influence mechanism of the building structure on the thermal environment. It was this strong influence of the 3D building structures on LST at the micro scale that makes it the most important factor affecting the community thermal environment. When the study scale was upgraded to the whole city, the 2D building morphological features tended to exert a greater impact on LST (Berger et al., 2017; Liu et al., 2021a,b; Yu et al., 2021).

Apart from spatial scales, different temporal scales could also lead to discrepancies in researchers' understanding of the relationship between landscape and thermal environment. Existing studies have investigated this relationship at the diurnal (Lai et al., 2021; Hesslerová et al., 2013), seasonal (Liu and Weng, 2008; Peng et al., 2018; Guha and Govil, 2022), and annual (Zhou et al., 2016; Dutta et al., 2019) scales and they have given a plenty of different and even opposite conclusions. This study further complemented some new findings on the relationship between landscape and thermal environment on a daily scale to help refine stakeholder perceptions.

5.2. Relationship between landscape, thermal environment and livability from different perspectives

This study introduced the concept of "thermal livability" to measure the stable comfort of a community's thermal environment, so as to analyze the optimal community landscape configuration that can maintain a livable thermal environment. Fig. 16 demonstrated an interesting finding: on most days, the average sky view factor of building (MEAN_SVF) in thermally livable communities is lower than that of other communities. Fig. S6 also exhibited that a smaller MEAN_SVF have a warming effect during high air pressure days, while the opposite was true in low air pressure days. Therefore, it can be inferred that a building structure with a lower MEAN_SVF is conducive to achieving a livable community thermal environment across summer and winter seasons since air pressure is generally lower in summer and higher in winter. This finding has also been witnessed in Kim et al. (2022b). However, some studies have put forward contradictory suggestions from the perspective of residents' subjective cognition on community livability. Sarkar et al. (2021) found through interviews that residents generally perceived communities with higher building SVF to be more livable because of more daylight and better air circulation. Guo et al. (2021) also pointed out that residents prefer community environments with open views when choosing where to live. A similarly controversial indicator was the volume ratio of building (PLOT_RATIO). The results in both Figs. 16 and S7 implied that higher PLOT_RATIO was more beneficial to constructing a livable community thermal environment. Nevertheless, in the general perception of community residents, the lower the PLOT_RATIO of a community, the higher its livability (Pandey et al., 2010). Thus, we can conclude that when treating a problem from different perspectives, the conclusions we obtained can vary enormously.

Beyond that, factors such as aesthetic significance, economic value, and social function are also essential for landscape planning and design, which requires planners to take a multifaceted consideration and trade-off to maximize the community livability. In this sense, the specific thresholds of landscape metrices that provided in this study can facilitate the formulation of urban renewal strategies from the perspective of improving the thermal livability of the communities.

6. Conclusion

The comfort of thermal environment is an important indicator for evaluating regional livability, but it has not yet received sufficient attention in existing studies. In this study, we designed a thermal livability index based on LST thresholds and used it as a bridge to link thermal environment and livability, elucidating two critical research issues: (1) the influence mechanism of landscape on thermal environment and its temporal variation at the community scale; and (2) the optimal community landscape configuration that is conducive to maintaining a livable thermal environment. The results revealed that landscape is not only an ornament of the city, but also a "regulator" between thermal environment and livability, which complemented the previous research results and provided planners with a new perspective from thermal livability when designing community landscapes.

Some limitations still remained in this study. It is well known that remotely sensed LST products usually have missing values due to cloud cover. Even though this study attempted to obtain as much available L2SPs as possible by extending the research period, there were still very few eligible data in some months (e.g., March, April and May). This may lead to bias in the data analysis for that month or affect the regularity of the continuous time series analysis. In addition, the results of this study were only applicable to Shenzhen city. The same approach may yield discrepant conclusions when applied to other cities, as the influence mechanism of landscape on the thermal environment tends to receive the impact of background climate and urban development level, which has been argued in previous studies. Nonetheless, the methodology proposed in this study provided new ideas and feasible technical routes to address some of the questions that remain (such as the two critical research issues mentioned above). In the next step, we will consider expanding the temporal and spatial scope of the study to obtain more generalized conclusions and reveal the characteristics of spatiotemporal variations.

CRediT authorship contribution statement

Yue Liu: Conceptualization, Methodology, Data analysis, Writing-Original draft preparation; **Xin Huang**: Data provider, Writing-Reviewing and Editing; **Qiquan Yang**: Conceptualization, Validation, Visualization; **Wenlong Jing**: Supervision, Writing- Reviewing and Editing; **Ji Yang**: Funding acquisition, Writing- Reviewing and Editing.

Declaration of competing interest

No conflict of interest exits in the submission of this manuscript, and manuscript is approved by all authors for publication. I would like to declare on behalf of my co-authors that the work described was original research that has not been published previously, and not under consideration for publication elsewhere, in whole or in part. All the authors listed have approved the manuscript that is enclosed.

Data availability

The data that has been used is confidential.

Acknowledgement

This research was supported by the National Natural Science Foundation of China under grants 41901372 and 41976189; the Guangdong Innovative and Entrepreneurial Research Team Program under grants 2016ZT06D336; the Science and Technology Program of Guangzhou under grants 202002030247; the GDAS' Project of Science and Technology Development under grants 2022GDASZH-2022010202; and the Science and Technology Program of Guangdong under grants 2021B1212100006.

Appendix A. Supplementary data

Supplementary data to this article can be found online at https://doi.org/10.1016/j.scitotenv.2023.167091.

References

Berger, C., Rosentreter, J., Voltersen, M., Baumgart, C., Schmullius, C., Hese, S., 2017. Spatio-temporal analysis of the relationship between 2D/3D urban site characteristics and land surface temperature. Remote Sens. Environ. 193, 225–243.

Breiman, L., 1996. Bagging predictors. Mach. Learn. 24 (2), 123–140.

Breiman, L., 2001. Random forests. Mach. Learn. 45 (1), 5–32.

Breiman, L., 2002. Manual on Setting Up, Using, and Understanding Random Forests v3. 1, 1(58). Statistics Department University of California Berkeley, CA, USA, pp. 3–42.

Cao, X., Onishi, A., Chen, J., Imura, H., 2010. Quantifying the cool island intensity of urban parks using ASTER and IKONOS data. Landsc. Urban Plan. 96 (4), 224–231.

Cao, J., Zhou, W., Zheng, Z., Ren, T., Wang, W., 2021. Within-city spatial and temporal heterogeneity of air temperature and its relationship with land surface temperature. Landsc. Urban Plan. 206, 103979.

de Freitas, C.R., Grigorieva, E.A., 2017. A comparison and appraisal of a comprehensive range of human thermal climate indices. Int. J. Biometeorol. 61, 487–512.

Deschenes, O., 2014. Temperature, human health, and adaptation: a review of the empirical literature. Energy Econ. 46, 606–619.

Dobrowski, S.Z., 2011. A climatic basis for microrefugia: the influence of terrain on climate. Glob. Chang. Biol. 17 (2), 1022–1035.

Dutta, D., Rahman, A., Paul, S.K., Kundu, A., 2019. Changing pattern of urban landscape and its effect on land surface temperature in and around Delhi. Environ. Monit. Assess. 191 (9), 1–15.

Gasparrini, A., Guo, Y., Hashizume, M., Lavigne, E., Zanobetti, A., Schwartz, J., Armstrong, B., 2015. Mortality risk attributable to high and low ambient temperature: a multicountry observational study. Lancet 386 (9991), 369–375.

Goldblatt, R., Addas, A., Crull, D., Maghrabi, A., Levin, G.G., Rubinyi, S., 2021. Remotely sensed derived land surface temperature (LST) as a proxy for air temperature and thermal comfort at a small geographical scale. Land 10 (4), 410.

Guha, S., Govil, H., 2022. Seasonal impact on the relationship between land surface temperature and normalized difference vegetation index in an urban landscape. Geocarto Int. 37 (8), 2252–2272.

Guo, A., Yang, J., Sun, W., Xiao, X., Cecilia, J.X., Jin, C., Li, X., 2020. Impact of urban morphology and landscape characteristics on spatiotemporal heterogeneity of land surface temperature. Sustain. Cities Soc. 63, 102443.

Guo, Y., Liu, Y., Lu, S., Chan, O.F., Chui, C.H.K., Lum, T.Y.S., 2021. Objective and perceived built environment, sense of community, and mental wellbeing in older adults in Hong Kong: a multilevel structural equation study. Landsc. Urban Plan. 209, 104058.

Hesslerová, P., Pokorný, J., Brom, J., Rejšková–Procházková, A., 2013. Daily dynamics of radiation surface temperature of different land cover types in a temperate cultural landscape: consequences for the local climate. Ecol. Eng. 54, 145–154.

Hou, H., Longyang, Q., Su, H., Zeng, R., Xu, T., Wang, Z.H., 2023a. Prioritizing environmental determinants of urban heat islands: a machine learning study for major cities in China. Int. J. Appl. Earth Obs. 122, 103411.

Hou, H., Su, H., Yao, C., Wang, Z.H., 2023b. Spatiotemporal patterns of the impact of surface roughness and morphology on urban heat island. Sustain. Cities Soc. 92, 104513.

Hsu, A., Sheriff, G., Chakraborty, T., Manya, D., 2021. Disproportionate exposure to urban heat island intensity across major US cities. Nat. Commun. 12 (1), 2721.

Huang, X., Liu, Y., 2022. Livability assessment of 101,630 communities in China's major cities: a remote sensing perspective. Sci. China Earth Sci. 65 (6), 1073–1087.

Huang, X., Wang, Y., 2019. Investigating the effects of 3D urban morphology on the surface urban heat island effect in urban functional zones by using high-resolution remote sensing data: a case study of Wuhan, Central China. ISPRS J. Photogramm. Remote Sens. 152, 119–131.

Huang, X., Wang, Y., Li, J., Chang, X., Cao, Y., Xie, J., Gong, J., 2020. High-resolution urban land-cover mapping and landscape analysis of the 42 major cities in China using ZY-3 satellite images. Sci. Bull. 65 (12), 1039–1048.

Keppel, G., Robinson, T.P., Wardell-Johnson, G.W., Yates, C.J., Van Niel, K.P., Byrne, M., Schut, A.G., 2017. A low-altitude mountain range as an important refugium for two narrow endemics in the Southwest Australian Floristic Region biodiversity hotspot. Ann. Bot. 119 (2), 289–300.

Kim, J., Lee, D.K., Kim, H.G., 2020. Suitable trees for urban landscapes in the Republic of Korea under climate change. Landsc. Urban Plan. 204, 103937.

Kim, J., Lee, D.K., Brown, R.D., Kim, S., Kim, J.H., Sung, S., 2022b. The effect of extremely low sky view factor on land surface temperatures in urban residential areas. Sustain. Cities Soc. 80, 103799.

Kim, Y., Yu, S., Li, D., Gatson, S.N., Brown, R.D., 2022a. Linking landscape spatial heterogeneity to urban heat island and outdoor human thermal comfort in Tokyo: application of the outdoor thermal comfort index. Sustain. Cities Soc. 87, 104262.

Kumar, P., Sharma, A., 2020. Study on importance, procedure, and scope of outdoor thermal comfort–A review. Sustain. Cities Soc. 61, 102297.

Lai, J., Zhan, W., Voogt, J., Quan, J., Huang, F., Zhou, J., Lee, X., 2021. Meteorological controls on daily variations of nighttime surface urban heat islands. Remote Sens. Environ. 253, 112198.

Larson, K.L., Andrade, R., Nelson, K.C., Wheeler, M.M., Engebreston, J.M., Hall, S.J., Trammell, T.L., 2020. Municipal regulation of residential landscapes across US cities: patterns and implications for landscape sustainability. J. Environ. Manag. 275, 111132.

Li, D., Liao, W., Rigden, A.J., Liu, X., Wang, D., Malyshev, S., Shevliakova, E., 2019. Urban heat island: aerodynamics or imperviousness? Sci. Adv. 5 (4) eaau4299.

Li, Y., Schubert, S., Kropp, J.P., Rybski, D., 2020. On the influence of density and morphology on the Urban Heat Island intensity. Nat. Commun. 11 (1), 2647.

Li, H., Li, Y., Wang, T., Wang, Z.H., Gao, M., Shen, H., 2021. Quantifying 3D building form effects on urban land surface temperature and modeling seasonal correlation patterns. Build. Environ. 204, 108132.

Liu, H., Weng, Q., 2008. Seasonal variations in the relationship between landscape pattern and land surface temperature in Indianapolis, USA. Environ. Monit. Assess. 144 (1), 199–219.

Liu, Y., Huang, X., Yang, Q., Cao, Y., 2021a. The turning point between urban vegetation and artificial surfaces for their competitive effect on land surface temperature. J. Clean. Prod. 292, 126034.

Liu, Y., Wang, Z., Liu, X., Zhang, B., 2021b. Complexity of the relationship between 2D/3D urban morphology and the land surface temperature: a multiscale perspective. Environ. Sci. Pollut. Res. 28 (47), 66804–66818.

McGarigal, K., Cushman, S.A., Ene, E., 2012. FRAGSTATS v4: spatial pattern analysis program for categorical and continuous maps. In: Computer Software Program Produced by the Authors at the University of Massachusetts, Amherst, 15.

O'Neill, R.V., Krummel, J.R., Gardner, R.E.A., Sugihara, G., Jackson, B., DeAngelis, D.L., Graham, R.L., 1988. Indices of landscape pattern. Landsc. Ecol. 1 (3), 153–162.

Pandey, R.U., Garg, Y.K., Bharat, A., 2010. A framework for evaluating residential built environment performance for livability. ITPI J. 7 (4), 12–20.

Peng, J., Jia, J., Liu, Y., Li, H., Wu, J., 2018. Seasonal contrast of the dominant factors for spatial distribution of land surface temperature in urban areas. Remote Sens. Environ. 215, 255–267.

Ramyar, R., Ackerman, A., Johnston, D.M., 2021. Adapting cities for climate change through urban green infrastructure planning. Cities 117, 103316.

Ruth, M., Franklin, R.S., 2014. Livability for all? Conceptual limits and practical implications. Appl. Geogr. 49, 18–23.

Sarkar, A., Kumar, N., Jana, A., Bardhan, R., 2021. Association Between Built-environment and Livability: Case of Mumbai Slum Rehabs. In: Urban Science and Engineering. Springer, Singapore, pp. 63–74.

Shiflett, S.A., Liang, L.L., Crum, S.M., Feyisa, G.L., Wang, J., Jenerette, G.D., 2017. Variation in the urban vegetation, surface temperature, air temperature nexus. Sci. Total Environ. 579, 495–505.

Suggitt, A.J., Wilson, R.J., Isaac, N.J., Beale, C.M., Auffret, A.G., August, T., Maclean, I. M., 2018. Extinction risk from climate change is reduced by microclimatic buffering. Nat. Clim. Chang. 8 (8), 713–717.

Tang, D., Gong, X., Liu, M., 2022. Residents' behavioral intention to participate in neighborhood micro-renewal based on an extended theory of planned behavior: a case study in Shanghai, China. Habitat Int. 129, 102672.

Tang, X., Zhou, P., Zhang, G., Wang, X., Jiang, Y., Guo, L., Liu, S., 2015. Verification of ZY-3 satellite imagery geometric accuracy without ground control points. IEEE Geosci. Remote Sens. Lett. 12 (10), 2100–2104.

Tong, M., She, J., Tan, J., Li, M., Ge, R., Gao, Y., 2020. Evaluating street greenery by multiple indicators using street-level imagery and satellite images: a case study in Nanjing, China. Forests 11 (12), 1347.

Turner, M.G., 1990. Spatial and temporal analysis of landscape patterns. Landsc. Ecol. 4 (1), 21–30.

Wang, C., Wang, Z.H., Wang, C., Myint, S.W., 2019. Environmental cooling provided by urban trees under extreme heat and cold waves in US cities. Remote Sens. Environ. 227, 28–43.

Xiao, J., Yuizono, T., 2022. Climate-adaptive landscape design: microclimate and thermal comfort regulation of station square in the Hokuriku Region, Japan. Build. Environ. 212, 108813.

Yang, Q., Huang, X., Yang, J., Liu, Y., 2021. The relationship between land surface temperature and artificial impervious surface fraction in 682 global cities: spatiotemporal variations and drivers. Environ. Res. Lett. 16 (2), 024032.

Yang, Q., Xu, Y., Tong, X., Huang, X., Liu, Y., Chakraborty, T.C., Hu, T., 2023. An adaptive synchronous extraction (ASE) method for estimating intensity and footprint of surface urban heat islands: a case study of 254 North American cities. Remote Sens. Environ. 297, 113777.

Yao, L., Li, T., Xu, M., Xu, Y., 2020. How the landscape features of urban green space impact seasonal land surface temperatures at a city-block-scale: an urban heat island study in Beijing, China. Urban For. Urban Green. 52, 126704.

Yao, R., Wang, L., Huang, X., Niu, Z., Liu, F., Wang, Q., 2017. Temporal trends of surface urban heat islands and associated determinants in major Chinese cities. Sci. Total Environ. 609, 742–754.

Yin, Q., Wang, J., Ren, Z., Li, J., Guo, Y., 2019. Mapping the increased minimum mortality temperatures in the context of global climate change. Nat. Commun. 10 (1), 1–8.

Yu, S., Chen, Z., Yu, B., Wang, L., Wu, B., Wu, J., Zhao, F., 2020. Exploring the relationship between 2D/3D landscape pattern and land surface temperature based on explainable eXtreme Gradient Boosting tree: a case study of Shanghai, China. Sci. Total Environ. 725, 138229.

Yu, X., Liu, Y., Zhang, Z., Xiao, R., 2021. Influences of buildings on urban heat island based on 3D landscape metrics: an investigation of China's 30 megacities at micro grid-cell scale and macro city scale. Landsc. Ecol. 36 (9), 2743–2762.

Yu, Z., Xu, S., Zhang, Y., Jørgensen, G., Vejre, H., 2018. Strong contributions of local background climate to the cooling effect of urban green vegetation. Sci. Rep. 8 (1), 6798.

Yuan, B., Zhou, L., Dang, X., Sun, D., Hu, F., Mu, H., 2021. Separate and combined effects of 3D building features and urban green space on land surface temperature. J. Environ. Manag. 295, 113116.

Zheng, Z., Zhou, W., Yan, J., Qian, Y., Wang, J., Li, W., 2019. The higher, the cooler? Effects of building height on land surface temperatures in residential areas of Beijing. Phys. Chem. Earth A/B/C 110, 149–156.

Zhou, D., Zhao, S., Zhang, L., Sun, G., Liu, Y., 2015. The footprint of urban heat island effect in China. Sci. Rep. 5 (1), 1–11.

Zhou, D., Zhang, L., Hao, L., Sun, G., Liu, Y., Zhu, C., 2016. Spatiotemporal trends of urban heat island effect along the urban development intensity gradient in China. Sci. Total Environ. 544, 617–626.
Zhou, D., Xiao, J., Bonafoni, S., Berger, C., Deilami, K., Zhou, Y., Sobrino, J.A., 2018. Satellite remote sensing of surface urban heat islands: progress, challenges, and perspectives. Remote Sens. 11 (1), 48.
Zhou, W., Wang, J., Cadenasso, M.L., 2017. Effects of the spatial configuration of trees on urban heat mitigation: a comparative study. Remote Sens. Environ. 195, 1–12.
Ziter, C.D., Pedersen, E.J., Kucharik, C.J., Turner, M.G., 2019. Scale-dependent interactions between tree canopy cover and impervious surfaces reduce daytime urban heat during summer. Proc. Natl. Acad. Sci. 116 (15), 7575–7580.